PHYSICAL REVIEW D **78,** 085019 (2008)

Virtual hadronic and heavy-fermion $\mathcal{O}(\alpha^2)$ corrections to Bhabha scattering

Stefano Actis,[1,*] Michał Czakon,[2,3,+] Janusz Gluza,[3,‡] and Tord Riemann[4,§]

[1]*Institut für Theoretische Physik E, RWTH Aachen University, D-52056 Aachen, Germany*
[2]*Institut für Theoretische Physik und Astrophysik, Universität Würzburg, Am Hubland, D-97074 Würzburg, Germany*
[3]*Institute of Physics, University of Silesia, Uniwersytecka 4, PL-40-007 Katowice, Poland*
[4]*DESY, Platanenallee 6, 15738 Zeuthen, Germany*

(Received 26 August 2008; published 23 October 2008)

Effects of vacuum polarization by hadronic and heavy-fermion insertions were the last unknown two-loop QED corrections to high-energy Bhabha scattering and have been announced in [S. Actis, M. Czakon, J. Gluza, and T. Riemann, Phys. Rev. Lett. **100**, 131602 (2008).]. Here we describe the corrections in detail and explore their numerical influence. The hadronic contributions to the virtual $\mathcal{O}(\alpha^2)$ QED corrections to the Bhabha-scattering cross section are evaluated using dispersion relations and computing the convolution of hadronic data with perturbatively calculated kernel functions. The technique of dispersion integrals is also employed to derive the virtual $\mathcal{O}(\alpha^2)$ corrections generated by muon-, tau-, and top-quark loops in the small electron-mass limit for arbitrary values of the internal-fermion masses. At a meson factory with 1 GeV center-of-mass energy the complete effect of hadronic and heavy-fermion corrections amounts to less than 0.5 per mille and reaches, at 10 GeV, up to about 2 per mille. At the Z resonance it amounts to 2.3 per mille at 3 degrees; overall, hadronic corrections are less than 4 per mille. For ILC energies (500 GeV or above), the combined effect of hadrons and heavy fermions becomes 6 per mille at 3 degrees; hadrons contribute less than 20 per mille in the whole angular region.

DOI: 10.1103/PhysRevD.78.085019 PACS numbers: 11.15.Bt, 12.20.Ds

I. INTRODUCTION

Elastic e^+e^- scattering, or Bhabha scattering,

$$e^-(p_1) + e^+(p_2) \to e^-(p_3) + e^+(p_4), \tag{1}$$

was one of the first scattering processes that were observed and predicted in quantum mechanics [1]. It has a unique and clean experimental signature. The accuracy of theoretical predictions profits from its purely leptonic external particle content and from the extremely small electron mass. The first complete one-loop prediction in the standard model was [2], the first $O(\alpha)$ predictions in the standard model with account of hard bremsstrahlung were determined in [3–8], the effects from hadronic vacuum polarization were first studied in [9], and the leading NNLO corrections from the top quark in [10]. The complete electroweak two-loop corrections are available in form of few form factors [11,12], but they are not implemented for Bhabha scattering so far. During the years, a rich literature on the subject arose, both concerning QED Monte Carlo results and virtual electroweak corrections; see [13–86], and also the references therein.

Quite recently, an experimental precision at the per mille level or beyond seems feasible both at meson factories and in the ILC (and GigaZ) project [87–92]. As a reaction to that, a program of systematic evaluation of the complete next-to-next-to leading order (NNLO) contributions was emerging [93–118].

In this article, we extensively describe the evaluation of the last building block of QED two-loop corrections, namely, the corrections from heavy fermions and hadronic vacuum polarization. Note that the latter result has been confirmed very recently in [119] (upon using the same parametrization of the vacuum polarization, the agreement between the two studies is perfect, 5 digits for the $\mathcal{O}(\alpha^4)$ NNLO terms). Both for reasons of completeness and in order to ensure easy comparisons, we will also include in the discussion the $N_f = 1$ corrections which consist of purely photonic corrections and electron-loop insertions, the soft bremsstrahlung and soft electron pair emission corrections. Concerning genuine two-loop effects, we take the results from the original computations of [100] (electron-loop corrections) and [104] (photonic corrections beyond logarithmic accuracy); soft electron pair emission is taken from the work of [44] (with logarithmic accuracy). All the two-loop contributions are calculated in our numerical Fortran package BHBHNNLOHF.F and will be made available at the webpage [120].

The organization of the paper is as follows. In Sec. II we introduce notations and the Born cross section. Section III collects the known facts on pure vacuum-polarization corrections as they will be used, and Sec. IV the pure self-energy corrections to the cross section. Section V contains the irreducible vertex corrections and Sec. VI the various infrared divergent corrections, including reducible corrections, soft-photon emission and the most complicated ones from the irreducible two-loop box diagrams. The three

*actis@physik.rwth-aachen.de
+mczakon@yahoo.com
‡gluza@us.edu.pl
§Tord.Riemann@desy.de

kernel functions for the latter have been evaluated for the first time. Section VII contains a discussion of numerical effects at a variety of energies, typical of meson factories, LEP, ILC. In the summary we will also point to potential further research. Appendices A to F are devoted to technical details of fermionic vacuum polarization, one-loop master integrals, soft real bremsstrahlung, real pair emission, the evaluation of the hadronic cross-section ratio R_{had}, and on our evaluation of complex polylogarithms. Some Mathematica files of potential public interest and the Fortran package are available at the webpage [120].

II. THE BORN CROSS SECTION

The QED tree-level differential Bhabha-scattering cross section with respect to the solid angle Ω, in the kinematic region $m_e^2 \ll s, |t|, |u|$, is:

$$\frac{d\sigma_0}{d\Omega} = \frac{\alpha^2}{2s}\left\{\frac{v_1(s,t)}{s^2} + 2\frac{v_2(s,t)}{st} + \frac{v_1(t,s)}{t^2}\right\} = \frac{\alpha^2}{s}\left(\frac{s}{t} + 1 + \frac{t}{s}\right)^2. \tag{2}$$

Here, α is the fine-structure constant [121],

$$\alpha = 1/137.035\,999\,679(94), \tag{3}$$

and

$$v_1(x,y) = x^2 + 2y^2 + 2xy, \tag{4}$$

$$v_2(x,y) = (x+y)^2. \tag{5}$$

The cross section depends on the Mandelstam invariants s, t and u, which are related to E, the incoming-particle energy in the center-of-mass frame, and θ, the scattering angle:

$$\begin{aligned} s &= (p_1 + p_2)^2 = 4E^2, \\ t &= (p_1 - p_3)^2 = -4E^2\sin^2\left(\frac{\theta}{2}\right), \\ u &= (p_1 - p_4)^2 = -4E^2\cos^2\left(\frac{\theta}{2}\right), \end{aligned} \tag{6}$$

where

$$s + t + u = 0. \tag{7}$$

For the numerical estimates at higher energies, it is reasonable to normalize the higher order corrections to the complete electroweak effective Born cross section:

$$\frac{d\sigma_{\mathrm{ew}}}{d\Omega} = \frac{\alpha^2}{4s}(T_s + T_{st} + T_t), \tag{8}$$

with

$$T_s = (1+\cos^2\theta)[1 + 2\mathrm{Re}\chi(s)(v^2) + |\chi(s)|^2(1+v^2)^2] + 2\cos\theta[2\mathrm{Re}\chi(s) + |\chi(s)|^2(4v^2)], \tag{9}$$

$$T_{st} = -2\frac{(1+\cos\theta)^2}{(1-\cos\theta)}\{1 + [\chi(t) + \mathrm{Re}\chi(s)](1+v^2) + \chi(t)\mathrm{Re}\chi(s)[(1+v^2)^2 + 4v^2]\}, \tag{10}$$

$$T_t = 2\frac{(1+\cos\theta)^2}{(1-\cos\theta)^2}\{1 + 2\chi(t)(1+v^2) + \chi(t)^2[(1+v^2)^2 + 4v^2]\} + \frac{8}{(1-\cos\theta)^2}[1 - \chi(t)(1-v^2)]^2. \tag{11}$$

We choose the following conventions:

$$v = 1 - 4s_w^2, \tag{12}$$

$$\chi(s) = \frac{G_F}{\sqrt{2}}\frac{M_Z^2}{8\pi\alpha}\frac{s}{s - M_Z^2 + iM_Z\Gamma_Z}, \tag{13}$$

$$\chi(t) = \frac{G_F}{\sqrt{2}}\frac{M_Z^2}{8\pi\alpha}\frac{t}{t - M_Z^2}. \tag{14}$$

Among the quantities α, G_F, s_w^2, M_Z there are only three independent, and Γ_Z is predicted by the theory as well. The phrasing *effective Born cross section* means here that we use, besides α [introduced in (3)], the following input variables:

$$s_w^2 = 0.23, \tag{15}$$

$$M_Z = 91.188\ \mathrm{GeV}, \tag{16}$$

$$\Gamma_Z = 2.495\ \mathrm{GeV}, \tag{17}$$

$$G_F = 1.166\,37 \times 10^{-5}\ \mathrm{GeV}^{-2}. \tag{18}$$

The values are, in a strict sense, related in the standard model, and may be determined e.g. by using the package ZFITTER [62,81]. Here, we took them from [121].

We may now estimate the relevance of the Z-boson exchange to Bhabha scattering in different kinematic regions of interest. It is minor at smallest energies where s, $|t| \ll M_Z^2$, because there $\chi(x) \sim x/M_Z^2 \ll 1$, $x = s, t$. The strength of the Z exchange amplitude, relative to the photon exchange, becomes at large s, $|t|$ asymptotically:

$$\frac{G_F}{\sqrt{2}}\frac{M_Z^2}{8\pi\alpha} = 0.3739. \tag{19}$$

The other scale of relevance here is the ratio of photon propagators in the s- and t-channels:

$$\frac{s}{t} = -\frac{2}{1-\cos\theta}. \tag{20}$$

In fact, at meson factory energies, the electroweak Born cross section agrees with the QED prediction within few per mille, and at LEP2 or the ILC within better than 50%, while at LEP1 or at GigaZ the ratio may become bigger

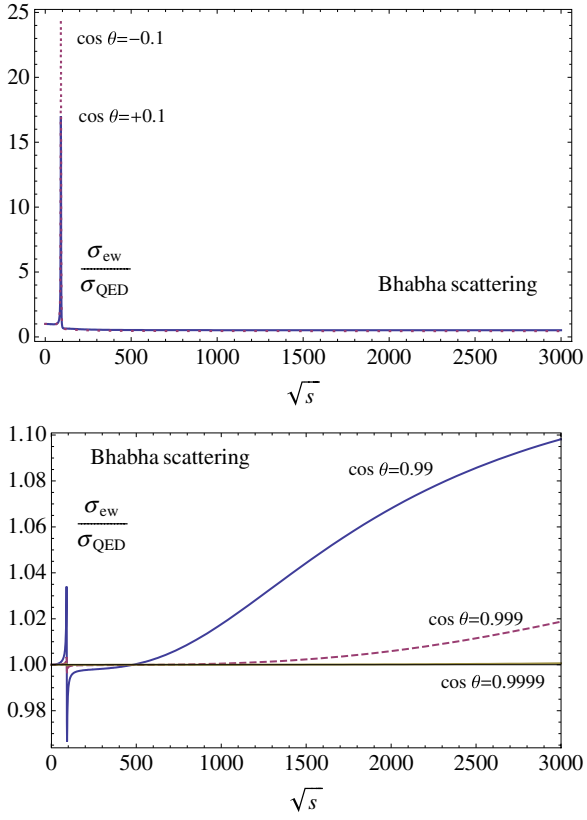

FIG. 1 (color online). Ratio of electroweak to QED Bhabha scattering cross section at large angles (up) and small angles (down) as a function of $\sqrt{s}$.

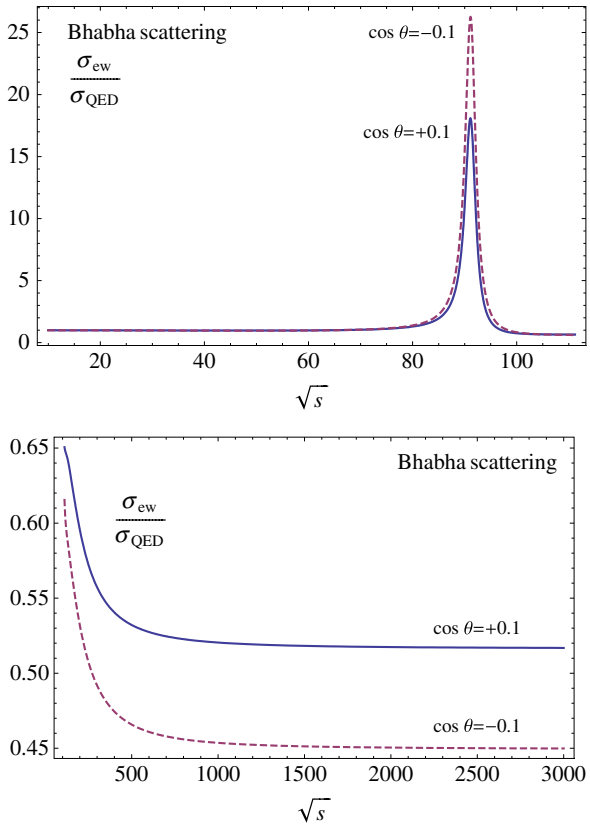

FIG. 2 (color online). Ratio of electroweak to QED Bhabha scattering cross section at large angles in the energy ranges of LEP1/GigaZ (up) and ILC (down).

than 25; this happens of course only for large scattering angles. At small angles, the corrections may safely be normalized to the QED Born cross section everywhere. The gross features are illustrated in Fig. 1 for large and small angle Bhabha scattering. For large angles, we show the cross-section ratio separately for LEP1/GigaZ and the ILC in Fig. 2. We conclude that only for large angles at LEP 1 energies it is better to relate the corrections from higher order contributions to the weak Born prediction, while for all other kinematics one may use the simple QED Born cross section.

III. THE VACUUM POLARIZATION

Higher-order fermionic corrections to the Bhabha-scattering cross section can be obtained inserting the renormalized irreducible photon vacuum-polarization function, Π, in the appropriate virtual-photon propagator,

$$\frac{g_{\mu\nu}}{q^2+i\delta} \to \frac{g_{\mu\alpha}}{q^2+i\delta}(q^2 g^{\alpha\beta} - q^\alpha q^\beta)\Pi(q^2)\frac{g_{\beta\nu}}{q^2+i\delta}. \tag{21}$$

Here q is the momentum carried by the virtual photon, $\delta \to 0_+$. The vacuum polarization Π can be represented by the once-subtracted dispersion integral [122]:

$$\Pi(q^2) = -\frac{q^2}{\pi}\int_{4M^2}^{\infty} dz \frac{\mathrm{Im}\Pi(z)}{z}\frac{1}{q^2 - z + i\delta}, \tag{22}$$

where the appropriate production threshold for the intermediate state in Π is located at $q^2 = 4M^2$. We leave as understood the subtraction at $q^2 = 0$ for the renormalized photon self-energy.

Contributions to Π arising from leptons and the top quark can be computed directly in perturbation theory, setting $M = m_f$ in Eq. (22), where m_f is the mass of the fermion appearing in the loop, and inserting the imaginary part of the analytic result for Π.

We have at one-loop accuracy:

$$\begin{aligned}\mathrm{Im}\Pi_f(z) = &-\left(\frac{\alpha}{\pi}\right)F_\epsilon\left(\frac{m_e^2}{m_f^2}\right)^\epsilon Q_f^2 C_f \theta(z-4m_f^2)\frac{\pi}{3} \\ &\times\left\{\frac{\beta_f(z)}{2}[3-\beta_f^2(z)] + \epsilon\beta_f(z)\left[3+\frac{3}{2}L_{\beta_f}(z)\right.\right. \\ &\left.\left. -\frac{4}{3}\beta_f^2(z) - \frac{\beta_f^2(z)}{2}L_{\beta_f}(z)\right]\right\} + \mathcal{O}(\alpha^2),\end{aligned} \tag{23}$$

where Q_f is the electric charge, $Q_f = -1$ for leptons, $Q_f = 2/3$ for up-type quarks and $Q_f = -1/3$ for down-type quarks, and C_f is the color factor, $C_f = 1$ for leptons

and $C_f = 3$ for quarks. In addition, we have introduced the θ function, $\theta(x) = 1$ for $x \geq 0$ and $\theta(x) = 0$ for $x < 0$, and the threshold factor,

$$\beta_f(z) = \sqrt{1 - 4\frac{m_f^2}{z}}, \tag{24}$$

$$L_{\beta_f}(z) = \ln\left(\frac{1 - \beta_f^2(z)}{4\beta_f^2(z)}\right). \tag{25}$$

The overall regularization-dependent factor reads as

$$F_\epsilon = \left(\frac{m_e^2 \pi e^{\gamma_E}}{\mu^2}\right)^{-\epsilon}, \tag{26}$$

where μ is the 't Hooft mass unit and γ_E is the Euler-Mascheroni constant.

The inclusion of the $\mathcal{O}(\epsilon)$ terms in Eq. (23) deserves a comment. These terms might play a role when combining $\mathrm{Im}\Pi_f$ with a pole term of another one-loop insertion in a reducible two-loop Feynman diagram. The Bhabha-scattering cross section we are going to consider is an infrared-finite quantity, provided one takes into account the real emission of soft photons. Therefore, when summing up all contributions, the result does not show any pole in the ϵ plane and all radiative corrections, including the one-loop photon self-energy, can be evaluated at $\mathcal{O}(\epsilon^0)$. However, we retain the higher ϵ order in Eq. (23) for comparing partial results with those of [113].

In contrast to leptons and the top quark, light-quark contributions get modified by low-energy strong-interaction effects, which cannot be computed using perturbative QCD. However, these contributions can be evaluated using the optical theorem [123]. After relating $\mathrm{Im}\Pi_{\mathrm{had}}$ to the hadronic cross-section ratio R_{had} [122],

$$\mathrm{Im}\,\Pi_{\mathrm{had}}(z) = -\frac{\alpha}{3} R_{\mathrm{had}}(z), \tag{27}$$

$$R_{\mathrm{had}}(z) = \frac{\sigma(\{e^+e^- \to \gamma^\star \to \mathrm{hadrons}\}; z)}{(4\pi\alpha^2)(3z)}, \tag{28}$$

$\mathrm{Im}\Pi_{\mathrm{had}}$ can be obtained from the experimental data for R_{had} in the low-energy region and around hadronic resonances, and the perturbative-QCD prediction in the remaining regions. The lower integration boundary is given by $M = m_\pi$, where m_π is the pion mass. For self-energy corrections to Bhabha scattering at one-loop order this was first employed in [13]. Two-loop applications, similar to our study, are the evaluation of the hadronic vertex correction [124] and of two-loop hadronic corrections to the lifetime of the muon [125]. The latter study faces quite similar technical problems to those met here, like the infrared divergency of single contributions and the existence of several scales.

For the fermionic and hadronic corrections to Bhabha scattering at one-loop accuracy, there is only the *self-energy diagram* shown in Fig. 3(c). The two-loop *irreducible* self-energy contributions have the topology shown in Fig. 3(c). One has additionally the four classes of *two-loop diagrams* shown in Fig. 4 The *reducible* self-energy [Fig. 4 (a)] and vertex [Fig. 4(b)] topologies are much easier to evaluate than the *irreducible* vertex [Fig. 4(c)] and box [Fig. 4(d)] topologies. In fact, only the two-loop boxes were unknown until quite recently.

The two-loop corrections have to be added with the loop-by-loop contributions (the interferences of the topologies of Fig. 3) and with the soft-photon corrections. All these terms will be discussed in the following sections.

To summarize this section, the hadronic and heavy-fermion corrections to the Bhabha-scattering cross section can be obtained by replacing appropriately the photon

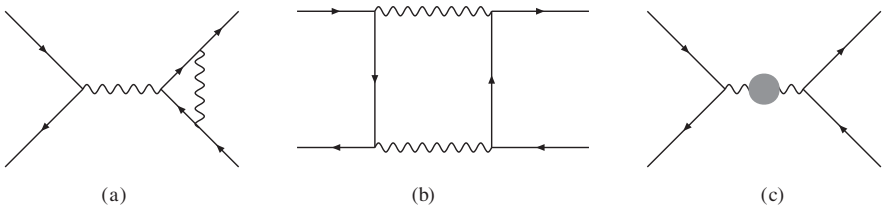

FIG. 3. The one-loop topologies for Bhabha scattering. The gray circle in (c) denotes the vacuum polarization under consideration, which may be understood to include fermionic and hadronic one- and two-loop irreducible self-energy corrections.

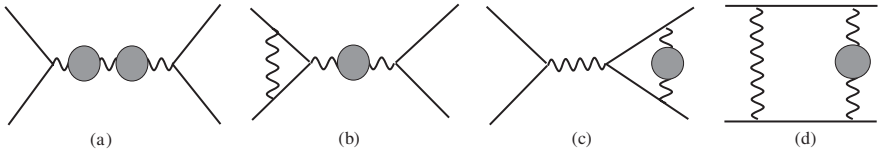

FIG. 4. Two-loop topologies for Bhabha scattering with vacuum polarization insertions: reducible self-energy (a) and vertex (b) corrections as well as irreducible vertex (c) and box (d) corrections; for the irreducible self-energy corrections see Fig. 3(c).

propagator by a massive propagator, whose effective mass z is subsequently integrated over. Inserting (22) and (27) in (21) we get:

$$\frac{g_{\mu\nu}}{q^2+i\delta} \to \frac{\alpha}{3\pi}\int_{4M^2}^{\infty} dz \frac{R(z)}{z}\frac{1}{q^2-z+i\delta}\left(g_{\mu\nu}-\frac{q_\mu q_\nu}{q^2+i\delta}\right). \tag{29}$$

In the following, we will call the massive propagator function in (29) the self-energy kernel function:

$$K_{\rm SE}(q^2;z) = \frac{1}{q^2-z+i\delta}. \tag{30}$$

The weight function $R(z)$ is given by the sum of the nonperturbative light-quark component of Eq. (28) and the perturbative result of Eq. (23), valid for leptons, $f = e$, μ, τ, and the top quark, $f = t$:

$$\begin{aligned} R(z) &= R^{(5)}_{\rm had}(z) - \frac{3}{\alpha}\sum_{f=e,\mu,\tau,t}{\rm Im}\Pi_f(z) \\ &= R^{(5)}_{\rm had}(z) + \sum_{f=e,\mu,\tau,t} R_f(z;m_f), \end{aligned} \tag{31}$$

$$R_f(z;m_f) = Q_f^2 C_f\left(1+2\frac{m_f^2}{z}\right)\sqrt{1-4\frac{m_f^2}{z}}. \tag{32}$$

Compared to (23), we omit here the terms of order $O(\epsilon)$. The function $R^{(5)}_{\rm had}(z)$ will be discussed in Appendix E.

Corrections related to electron insertions ($f = e$) will be discussed separately. For pure self-energy insertions (see Appendix A), we may consider the electron mass as being small and neglect terms of order $O(m_e^2/x)$, $x = s$, $|t|$, $|u|$. At the expense of that, even the three-loop corrections are known [126]. For two-loop irreducible vertex and box corrections, we may either consider m_e being finite and treat a two-scale problem (s/m_e^2, t/m_e^2), or we may assume also here $m_e^2 \ll s$, $|t|$, $|u|$. Instead, for the diagrams with self-energy insertions of other fermions f, we will assume $m_e^2 \ll m_f^2$, s, $|t|$, $|u|$, but we will make no additional assumption on m_f^2.

IV. PURE SELF-ENERGY CORRECTIONS

The pure vacuum-polarization contributions to Bhabha scattering form a gauge-invariant subset of diagrams. So, their numerics may be discussed separately. They can be readily obtained from the tree-level result (2) by introducing appropriately a running fine-structure constant $\alpha(x)$, where $x = s$, t,

$$\begin{aligned} \frac{d\sigma_{\alpha\rm run}}{d\Omega} = \frac{1}{2s}\Bigg[&|\alpha(s)|^2\frac{v_1(s,t)}{s^2} + 2\alpha(t){\rm Re}\alpha(s)\frac{v_2(s,t)}{st} \\ &+ \alpha^2(t)\frac{v_1(t,s)}{t^2}\Bigg] + \mathcal{O}(m_e^2), \end{aligned} \tag{33}$$

and where the running of α is defined as

$$\alpha(x) = \frac{\alpha}{1-\Delta\alpha(x)}. \tag{34}$$

Here $\Delta\alpha$ is given by the sum of the nonperturbative light-quark contribution $\Delta\alpha^{(5)}_{\rm had}$ [127] (see Refs. [128–130] and references therein for recent developments), a perturbative electron-loop component evaluated in the small electron-mass limit, Π_e, and a fermion-loop term computed exactly, Π_f, with $f = \mu$, τ, t,

$$\Delta\alpha(x) = \Delta\alpha^{(5)}_{\rm had}(x) + \Pi_e(x) + \sum_{f=\mu,\tau,t}\Pi_f(x), \tag{35}$$

$$\Delta\alpha^{(5)}_{\rm had}(x) = \frac{\alpha}{\pi}\frac{x}{3}\int_{4m_\pi^2}^{\infty} dz \frac{R^{(5)}_{\rm had}(z)}{z}K_{\rm SE}(x;z), \tag{36}$$

with the self-energy kernel function $K_{\rm SE}(x;z)$ (30).

For $x < 4m_\pi^2$, Eq. (36) is well defined. For $x > 4m_\pi^2$, the real and imaginary parts are after a subtraction:

TABLE I. Contributions to $\Delta\alpha$ in units of 10^{-4} in the s-channel [see Eq. (35)]. The real part of the hadronic contributions is obtained with help of the subroutine hadr5.f [132], the imaginary part follows from the Burkhardt parametrization [133].

$\sqrt{s}$ [GeV]	1	10	M_Z	500
1 loop e	104.462–24.3245i	140.119–24.3245i	174.347–24.3245i	200.698–24.3245i
μ	21.352–24.3060i	57.551–24.3245i	91.784–24.3245i	118.136–24.3245i
τ	−0.508	12.194–24.1724i	48.060–24.3245i	74.429–24.3245i
t	$<10^{-3}$	−0.007	−0.595	−5.180–29.0633i
2 loops e	0.258–0.0424i	0.320–0.0424i	0.380–0.0424i	0.426–0.0424i
μ	0.123–0.0487i	0.177–0.0424i	0.236–0.0424i	0.282–0.0424i
τ	−0.005	0.118–0.0626i	0.160–0.0426i	0.206–0.0424i
t	$<10^{-3}$	$<10^{-3}$	−0.002	0.061–0.0876i
3 loops e	0.001–0.0005i	0.002–0.0006i	0.003–0.0008i	0.004–0.0009i
hadrons	−74.420–37.9089i	138.850–97.4106i	276.213–97.2980i	370.744–97.2980i
SUM	51.263–86.6310i	349.324–170.3800i	590.586–170.3997i	759.806–199.5505i

TABLE II. Contributions to $\Delta\alpha$ in units of 10^{-4} in the t-channel for three values of the scattering angle, $\theta = 3°$, $\theta = 20°$ and $\theta = 90°$, $t = -s\sin^2(\theta/2)$. See the caption of Table I for further details.

$\theta[°]\|\sqrt{s}$ [GeV]	$\theta = 20\|1$	$\theta = 20\|1$	$\theta = 3\|M_Z$	$\theta = 3\|500$
1 loop e	77.3512	113.008	117.935	144.286
μ	3.3069	30.614	35.463	61.727
τ	0.0148	1.346	2.365	18.804
t	$<10^{-4}$	$<10^{-3}$	$<10^{-3}$	0.012
2 loops e	0.2109	0.273	0.282	0.327
μ	0.0260	0.126	0.136	0.184
τ	0.0001	0.011	0.019	0.097
t	$<10^{-4}$	$<10^{-3}$	$<10^{-3}$	$<10^{-3}$
3 loops e	0.0006	0.001	0.001	0.002
hadrons	2.6072	57.830	71.643	162.280
SUM	83.5177	203.209	227.844	387.719
$\theta = 90°\|\sqrt{s}$ [GeV]	1	10	M_Z	500
1 loop e	99.0951	134.752	168.980	195.331
μ	17.4725	52.200	86.418	112.769
τ	0.2412	10.841	42.746	69.064
t	$<10^{-4}$	0.003	0.284	6.208
2 loops e	0.2487	0.311	0.370	0.416
μ	0.0924	0.167	0.227	0.273
τ	0.0021	0.068	0.150	0.196
t	$<10^{-4}$	$<10^{-3}$	0.001	0.021
3 loops e	0.0009	0.002	0.003	0.003
hadrons	25.0834	127.219	256.279	362.375
SUM	142.2363	492.396	555.458	746.656

$$\mathrm{Re}\,[\Delta\alpha^{(5)}_{\mathrm{had}}(x)] = \frac{\alpha}{\pi}\frac{x}{3}\int_{4m_\pi^2}^{\infty} dz\,\frac{[R^{(5)}_{\mathrm{had}}(z) - R^{(5)}_{\mathrm{had}}(x)]}{z(x-z)} + \frac{\alpha}{3\pi}R^{(5)}_{\mathrm{had}}(x)\log\left[\frac{x}{4m_\pi^2} - 1\right], \quad (37)$$

$$\mathrm{Im}\,[\Delta\alpha^{(5)}_{\mathrm{had}}(x)] = -\frac{\alpha}{3}R^{(5)}_{\mathrm{had}}(x). \quad (38)$$

The $\mathrm{Im}[\Delta\alpha^{(5)}_{\mathrm{had}}(x)]$ coincides with Eq. (27). Expressions for the perturbative contributions to the photon vacuum-polarization function, Π_f and Π_e, are available in QED exactly up to two loops [131] and in the small electron-mass limit up to three loops [126]. For convenience, their explicit expressions are collected in Appendix A. For our analysis, we use the exact results of Eqs. (A3) and (A4) for fermion loops ($f \neq e$), and the high-energy expressions of Eqs. (A8)–(A10) for electron loops.

In Tables I and II we show numerical values for the various components of $\Delta\alpha$ of Eq. (35) for spacelike and timelike values of x (t- and s-channel). Note that $\Delta\alpha$ develops an imaginary part in the s-channel above the two-particle production threshold (see Table I). Besides the Fortran package HADR5.F for hadronic contributions [132], we employed the Mathematica package HPL [134,135] and, as a cross check, our Fortran routines (see Appendices A and F).

V. IRREDUCIBLE VERTEX CORRECTIONS

Hadronic and heavy-fermion irreducible vertex corrections are obtained through the interference of the diagrams of Fig. 5 with the tree-level amplitude. The contributions

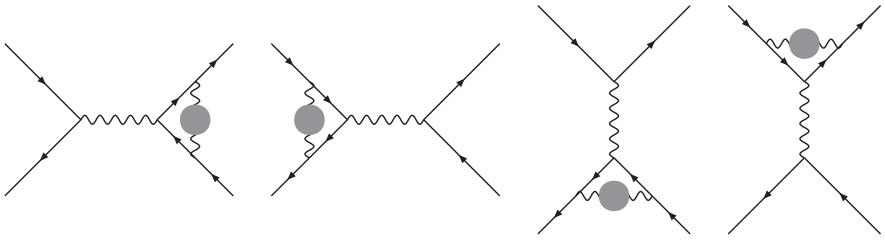

FIG. 5. Hadronic and fermionic irreducible vertex diagrams. The gray circles mark the corresponding one-loop insertions.

from the irreducible vertices are gauge invariant by themselves. Their contribution to the $\mathcal{O}(\alpha^2)$ differential cross section is given by

$$\frac{d\sigma_{\rm vert}}{d\Omega} = 4\left(\frac{\alpha}{\pi}\right)^2\left(\frac{\alpha^2}{2s}\right)\left\{\frac{v_1(s,t)}{s^2}\,{\rm Re}V_2(s) + \frac{v_1(t,s)}{t^2}V_2(t) + \frac{v_2(s,t)}{st}[{\rm Re}V_2(s) + V_2(t)]\right\} + \mathcal{O}(m_e^2). \quad (39)$$

Here V_2 summarizes all two-loop fermionic corrections to the QED Dirac form factor, whose computation can be traced back to the seminal work of Refs. [136,137]. The full result can be organized as

$$V_2(x) = V_{2e}(x) + V_{2\rm rest}(x), \quad (40)$$

where V_{2e} denotes the electron-loop component. Closed analytical expressions in the case of electron loops at finite m_e can be found in Ref. [97]. In the high-energy limit, compact expressions are available thanks to Ref. [138]:

$$V_{2e}(x) = \frac{1}{36}\ln^3\left(-\frac{m_e^2}{x}\right) + \frac{19}{72}\ln^2\left(-\frac{m_e^2}{x}\right) + \frac{1}{6}\left(\frac{265}{36} + \zeta_2\right)\ln\left(-\frac{m_e^2}{x}\right) + \frac{1}{4}\left(\frac{383}{27} - \zeta_2\right) + \mathcal{O}(m_e^2). \quad (41)$$

After a combination with soft real electron pair emission contributions (D1), the leading logarithmic contributions $\ln^3(s/m_e^2)$ get canceled in (39).

Heavy-fermion and hadronic contributions, instead, can be evaluated as in Ref. [124] through the dispersion integral

$$V_{2\rm rest}(x) = \int_{4M^2}^{\infty} dz\,\frac{R(z)}{z}K_V(x + i\delta; z), \quad (42)$$

where R is given in Eq. (31) and the two-loop irreducible vertex kernel function K_V, in the limit of a vanishing electron mass, reads as

$$K_V(x;z) = \frac{1}{3}\left\{-\frac{7}{8} - \frac{z}{2x} + \left(\frac{3}{4} + \frac{z}{2x}\right)\ln\left(-\frac{x}{z}\right) - \frac{1}{2}\left(1 + \frac{z}{x}\right)^2\left[\zeta_2 - {\rm Li}_2\left(1 + \frac{x}{z}\right)\right]\right\}. \quad (43)$$

Here ${\rm Li}_2(x)$ is the usual dilogarithm and $\zeta_2 = {\rm Li}_2(1) = \pi^2 6$. The kernel is at the upper integration boundary of the order $O(1/z)$, the integrand of order $O(1/z^2)$ so that the dispersion integral is finite there:

$$K_V(x;z) \approx \tfrac{1}{3}\{\tfrac{11}{36}u - \tfrac{1}{6}u\ln(-u) + (-\tfrac{13}{288} + \tfrac{1}{24}\ln(-u))u^2 + (\tfrac{47}{3600} - \tfrac{1}{60}\ln(-u))u^3\} \quad \text{for } u = \frac{x}{z} \to 0. \quad (44)$$

At the lower integration bound, the integrand becomes for small z/x:

$$K_V(x;z) \approx \frac{1}{3}\left\{-\frac{7}{8} - \zeta(2) + \frac{3}{4}\ln(-u) - \frac{1}{4}\ln^2(-u) - \left[1 + 2\zeta(2) + \frac{1}{2}\ln^2(-u)\right]\frac{1}{u}\right\} \quad \text{for } u = \frac{x}{z} \to \infty. \quad (45)$$

This asymptotic behavior yields at most terms of the order of $\ln^3(x/M^2)$ if $M^2 \ll x$.

An interesting question is the identification of mass logarithms in case of fermion insertions. Let us rewrite:

$$V_{2\rm rest}(x) = V_{2\rm had}^{(5)}(x) + \sum_{f=\mu,\tau,t} Q_f^2 C_f V_{2f}(x), \quad (46)$$

where $V_{2\rm had}^{(5)}$ denotes the nonperturbative light-quark term and V_{2f} the perturbative contribution of a fermion of flavor $f \neq e$. Potentially large logarithms arise from parts of the integrand for the z integration which are singular at the lower integration bound, $z \to 4M^2$, when allowing thereby M^2 to become small. For fermions, one has to analyze $R_f(z)K_V(x;z)/z$ in that limit.

The corresponding analytical integrations may be performed easily after applying the transformation

$$z = \frac{4m_f^2}{1-u^2}, \quad (47)$$

thereby getting rid of the square root function in $R_f(z)$:

$$R_f(z) = C_f Q_f^2 \frac{u}{2}(3 - u^2). \quad (48)$$

After that transformation, the dispersion integral becomes:

$$V_{2f}(x) = \int_0^1 du\left[-2 + u^2 + \frac{1}{1-u} + \frac{1}{1+u}\right] \times K_V\left(x + i\delta; \frac{4m_f^2}{1-u^2}\right). \quad (49)$$

From the vertex kernel function $K_V(x;z)$, we have additionally dependences on $\ln(-x/z)$ and on ${\rm Li}_2(1 + x/z)$. Although after the variable change (47) the arguments of logarithm and dilogarithm become nonlinear, all the integrals may be taken trivially, and we will not go into further details. The result contains ${\rm Li}_3$ and powers of logarithms $\ln^n(x/m_f^2)$ with $n \leq 3$. In fact, one will rediscover in the kinematically interesting ultrarelativistic case the formula known from [138] and e.g. also from [113]:

$$V_{2f}(x) = \frac{1}{36}\ln^3\left(-\frac{m_f^2}{x}\right) + \frac{19}{72}\ln^2\left(-\frac{m_f^2}{x}\right) + \frac{1}{6}\left(\frac{265}{36} + \zeta_2\right)\ln\left(-\frac{m_f^2}{x}\right) + \frac{1}{6}\left(\frac{3355}{216} + \frac{19}{6}\zeta_2 - 2\zeta_3\right) + \mathcal{O}(m_f^2). \quad (50)$$

The same soft- real pair cancellation mechanism as de-

scribed for electrons works also for heavy fermions, and the leading logarithmic powers $\ln^3(s/m_f^2)$ will get canceled in the cross section. This is of physical relevance if the soft pair emissions remain unobserved. In our numerical studies, we will, conventionally, include the soft electron pair emission cross section, but not that for heavy fermions or hadrons. For further details see Section D, and some numerical results were presented in [139], where we used the parametrization [133] with flag setting IPAR = 1.

We just mention that the transformation (47), when applied to the simple one-loop self-energy kernel (30),

$$K_{\mathrm{SE}}(x;z) = \frac{1}{x-z} = \frac{1}{x}\left[1 + \frac{4m_f^2/x}{1-u^2-4m_f^2/x}\right], \quad (51)$$

gives a rational integrand for the u-integration, and one gets as a result a function at most linear in $\ln(s/m_f^2)$. For the explicit expressions see Eqs. (A3) (constant term in ϵ) and (A8).

VI. INFRARED-DIVERGENT CORRECTIONS

There are various origins of heavy-fermion or hadronic infrared divergent cross-section contributions of order $O(\alpha^4)$:

(i) Factorizable diagrams with one-loop vertex or box insertions
(ii) Irreducible two-loop box diagrams
(iii) soft real photon corrections

The sum of these corrections is gauge-invariant and infrared finite.

We will consider five classes of contributions:

(a) Interference of Born diagrams with reducible [vertex+self-energy] corrections of Fig. 6;
(b) Interference of one-loop vertex and self-energy diagrams, both of Fig. 3;
(c) Interference of one-loop box and self-energy diagrams, both of Fig. 3;
(d) Interference of real soft-photon emission diagrams, one of them with a self-energy insertion;

(box) Interference of Born diagrams with two-loop box diagrams of Fig. 7.

For ease of notation, in the following we collect the overall dependence on α and rewrite the factorizing contributions of class i, $i = a, \ldots, d$:

$$\frac{d\sigma^i_{\mathrm{fact}}}{d\Omega} = \left(\frac{\alpha}{\pi}\right)^2 \frac{\alpha^2}{s} \frac{d\bar{\sigma}^i_{\mathrm{fact}}}{d\Omega}, \quad (52)$$

and analogously for the two-loop boxes. In addition, we define

$$\hat{s} = \frac{s}{m_e^2}, \quad (53)$$

$$r = -\frac{t}{s}, \quad (54)$$

and introduce shorthand notations for those kinematic factors which appear more than once in the following formulas:

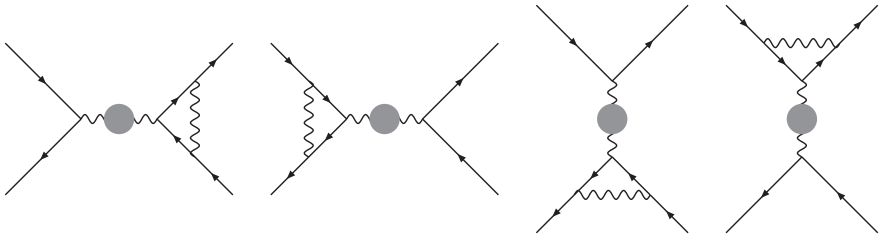

FIG. 6. Hadronic and fermionic reducible vertex diagrams. The gray circles mark the corresponding one-loop insertions.

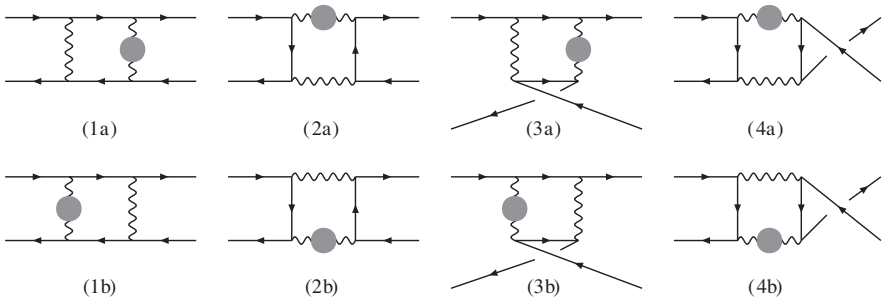

FIG. 7. Irreducible box diagrams. The gray circle denotes the hadronic or fermionic insertions.

$$A_r = -\frac{v_1(s,t)}{s^2} - \frac{v_2(s,t)}{st} = \frac{1}{r}[(1-r)^3 - r^3],$$
$$B_r = \frac{v_1(t,s)}{t^2} + \frac{v_2(s,t)}{st} = \frac{1}{r^2}[2(1-r)^2 + r(1+r-r^2)],$$
$$C_r = \frac{v_1(s,t)}{s^2} = (1-r)^2 + r^2,$$
$$D_r = -\frac{v_2(s,t)}{st} = \frac{1}{r}(1-r)^2,$$
$$E_r = 3\frac{v_1(t,s)}{t^2} + \frac{v_2(s,t)}{st} = \frac{1}{r^2}[6(1-r)^2 + r(5-r-r^2)],$$
$$F_r = \frac{1}{2}\frac{v_1(t,s)}{t^2} + \frac{1}{4}\frac{v_2(s,t)}{st} = \frac{1}{4r^2}[4(1-r)^2 + r(3-r^2)],$$
$$G_r = \frac{v_1(t,s)}{t^2} = \frac{1}{r^2}(1+(1-r)^2). \quad (55)$$

A. Factorizable corrections with vertex or box insertions

The infrared-divergent factorizable heavy fermion and hadronic corrections for $m_e^2 \ll M^2, s, |t|, |u|$ can be readily obtained from Ref. [113] by replacing the photon vacuum-polarization function in the s- or t-channel with the dispersion integral

$$\Pi(x) = \Delta\alpha(x) = \frac{\alpha}{\pi} I(x), \quad (56)$$

$$I(x) = \frac{x}{3}\int_{4M^2}^{\infty} \frac{dz}{z}\frac{R(z)}{x - z + i\delta}, \qquad x = s, t, \quad (57)$$

where $\Delta\alpha(x)$ is given in (35) and R in (31).

We begin with the reducible vertex corrections (a). From Eq. (3.8) of Ref. [113] we derive:

$$\frac{d\bar{\sigma}^a_{\rm fact}}{d\Omega} = \frac{F_\epsilon}{\epsilon}\{A_r[(1-\ln(\hat{s}))\mathrm{Re}I(s) - \pi\mathrm{Im}I(s)] + B_r[\ln(\hat{s}) + \ln(r) - 1]I(t)\} + \frac{1}{2}\{A_r[\ln^2(\hat{s}) - 8\zeta_2] - (A_r - 2C_r)\ln(\hat{s}) + 2(A_r - C_r)\}\mathrm{Re}I(s) + \frac{1}{2}[2A_r\ln(\hat{s}) - A_r + 2C_r]\pi\mathrm{Im}I(s) - \frac{1}{2}\{B_r[\ln^2(\hat{s}) + \ln^2(r)] - [E_r - 2B_r\ln(r)]\ln(\hat{s}) - E_r\ln(r) - 2B_r\zeta_2 + 8F_r\}I(t), \quad (58)$$

where the normalization factor F_ϵ is given in Eq. (26). It appears here in the combination

$$\frac{F_\epsilon}{\epsilon} = \frac{1}{\epsilon} - \ln\left(\frac{m_e^2}{\mu^2}\right) - \ln(\pi) - \gamma_E + \mathcal{O}(\epsilon). \quad (59)$$

In strict analogy, the interference of the one-loop vertex diagrams of Fig. 3(a), with the vacuum-polarization diagrams of Fig. 3(c) can be extracted from Eq. (3.26) of Ref. [113]:

$$\frac{d\bar{\sigma}^b_{\rm fact}}{d\Omega} = \frac{F_\epsilon}{\epsilon}\{[A_r(1-\ln(\hat{s})) - D_r\ln(r)]\mathrm{Re}I(s) - C_r\pi\mathrm{Im}I(s) + [B_r(\ln(\hat{s}) - 1) + G_r\ln(r)]I(t)\} + \frac{1}{2}\{A_r\ln^2(\hat{s}) - 2[(1-4r)D_r - 4r^2]\zeta_2 - [A_r - 2C_r - 2D_r\ln(r)]\ln(\hat{s}) + D_r\ln^2(r) - (D_r - 2)\ln(r) + 2[(1-2r)D_r - 2r^2]\}\mathrm{Re}I(s) + \frac{1}{2}\{2C_r\ln(\hat{s}) - [C_r - 4r(1-r)]\}\pi\mathrm{Im}I(s) - \frac{1}{2}\left\{B_r\ln^2(\hat{s}) - \left[E_r - \frac{2}{r^2}(1+rD_r)\ln(r)\right]\ln(\hat{s}) + \frac{1}{r^2}(1+rD_r)\ln^2(r) - \frac{1}{r^2}[6(1-r) + r^2]\ln(r) - \frac{2}{r^2}[r(1-4r)D_r + 1]\zeta_2 + 8F_r\right\}I(t). \quad (60)$$

Finally, the contributions from the one-loop box diagrams of Fig. 3(b) may be derived from Eq. (3.28) of Ref. [113]:

$$\frac{d\bar{\sigma}^c_{\rm fact}}{d\Omega} = \frac{F_\epsilon}{\epsilon}\{[C_r\ln(r) + A_r\ln(1-r)]\mathrm{Re}I(s) + D_r\pi\mathrm{Im}I(s) - [D_r\ln(r) + B_r\ln(1-r)]I(t)\} - \left\{[C_r\ln(r) + A_r\ln(1-r)]\ln(\hat{s}) + \ln(r) + \frac{1}{2}(2D_r + r)\ln(1-r) + \frac{3}{4}(1-r)\ln^2(r) + \frac{1}{4}(1-2r)\ln^2(1-r) + D_r\ln(r)\ln(1-r)\right\}\mathrm{Re}I(s) - \left\{D_r\ln(\hat{s}) + \frac{1}{2r}[D_r r(1-r) + 1 - 3r^3]\ln(r) + \frac{1}{2}[3(1-2r) + 4r^2]\ln(1-r) + \frac{1}{2r}(rD_r + 1 + 2r^2)\right\}\pi\mathrm{Im}I(s) + \left\{[D_r\ln(r) + B_r\ln(1-r)]\ln(\hat{s}) + \frac{1}{2r}(C_r + 2)\ln(r) - \frac{1}{2r}[rD_r + 2(1-r) + r^2]\ln(1-r) + \frac{1}{4r}(5-4r)\ln^2(r) + \frac{1}{4r}(2-r)\ln^2(1-r) + \frac{1}{2r^2}[2rD_r + 2(1-r) + r^2]\ln(r)\ln(1-r) + \frac{3}{2r}(2-r)\zeta_2\right\}I(t). \quad (61)$$

All three types of corrections are infrared divergent. The vertex diagrams contribute leading electron-mass singularities of the order $\ln^2(s/m_e^2)$, while for the factorizable box diagrams the leading order is $\ln(s/m_e^2)$. In addition, the self-energy insertions $I(x)$ yield a dependence on $\ln(s/m_f^2)$, in case m_f^2 is small compared to s. This may be most easily seen from the ϵ-independent terms in (A3). So, we collect here at most terms of the order $\ln^2(s/m_e^2)\ln(s/m_f^2)$.

B. Soft real photon emission

In order to obtain an infrared-finite quantity, we take into account the interferences of diagrams with real emission of soft photons from the external legs, where one of the diagram has a vacuum-polarization insertion. The anatomy of these real corrections is exemplified in Appendix C, where the soft photon factor is shown both for nonvanishing electron mass m_e and in the ultrarelativistic approximation. The result may be also read off from Eq. (4.4) of Ref. [113] and reads as

$$\frac{d\bar{\sigma}^{d}_{\text{fact}}}{d\Omega} = \frac{d\bar{\sigma}^{d,1}_{\text{fact}}}{d\Omega} + \ln\left(\frac{2\omega}{\sqrt{s}}\right)\frac{d\bar{\sigma}^{d,2}_{\text{fact}}}{d\Omega}, \tag{62}$$

where ω is the maximum energy carried by a soft photon in the final state. We obtain

$$\begin{aligned}\frac{d\bar{\sigma}^{d,1}_{\text{fact}}}{d\Omega} = {} & \frac{F_\epsilon}{\epsilon}2[\ln(\hat{s}) + \ln(r) - \ln(1-r) - 1][A_r\text{Re}I(s) - B_r I(t)] \\ & - 2\Big\{\Big[\frac{1}{2}\ln^2(\hat{s}) + \ln(\hat{s})(\ln(r) - \ln(1-r)) + \frac{1}{2}\ln^2(r) - \frac{1}{2}\ln^2(1-r) - \ln(r)\ln(1-r) - 2\text{Li}_2(r) - \zeta_2\Big] \\ & \times [A_r\text{Re}I(s) - B_r I(t)] + D_r[\ln(\hat{s}) + \ln(r) - \ln(1-r) - 1][\text{Re}I(s) + I(t)]\Big\},\end{aligned} \tag{63}$$

$$\frac{d\bar{\sigma}^{d,2}_{\text{fact}}}{d\Omega} = -4[\ln(\hat{s}) + \ln(r) - \ln(1-r) - 1][A_r\text{Re}I(s) - B_r I(t)]. \tag{64}$$

Again, the infrared divergency is contained in the factor F_ϵ/ϵ, and the mass singularities are at most of the orders $\ln(x/m_f^2)$, $x = s, t$, and $\ln^2(x/m_e^2)$ for the ω-independent part and $\ln(x/m_e^2)$ for the ω-dependent part.

C. Two-loop irreducible box corrections

From the technical point of view, the two-loop irreducible box corrections of this section, represented by the three box kernel functions, are the main result of the article. Their contributions to the Bhabha-scattering cross section arise from the interference of the diagrams of Fig. 7 with the tree-level amplitude and can be written as

$$\frac{d\sigma_{\text{box}}}{d\Omega} = \left(\frac{\alpha}{\pi}\right)^2\frac{\alpha^2}{s}\frac{d\bar{\sigma}_{\text{box}}}{d\Omega} = \left(\frac{\alpha}{\pi}\right)^2\frac{\alpha^2}{4s}2\left(\frac{\text{Re}A_s}{s} + \frac{\text{Re}A_t}{t}\right). \tag{65}$$

Here the functions A_s and A_t contain the interferences of box diagrams with the s-channel and t-channel tree-level diagrams and can be represented through three independent form factors, evaluated with different kinematic arguments:

$$A_s = B_A(s,t) + B_B(t,s) + B_C(u,t) - B_B(u,s), \tag{66}$$

$$A_t = B_B(s,t) + B_A(t,s) - B_B(u,t) + B_C(u,s). \tag{67}$$

In addition, note that in Eq. (65) we have collected an overall factor $1/4$, coming from the sum over the spins, and a factor 2, taking into account the fact that the contributions generated by the diagrams (1a), (2a), (3a) and (4a) are equivalent to those of diagrams (1b), (2b), (3b) and (4b) of Fig. 7. Finally, the correspondence among the form factors of Eq. (66) and the diagrams of Fig. 7 reads as follows:

$$\begin{aligned}&\text{diag1} \times \text{tree}_s \Rightarrow B_A(s,t), && \text{diag1} \times \text{tree}_t \Rightarrow B_B(s,t), \\ &\text{diag2} \times \text{tree}_s \Rightarrow B_B(t,s), && \text{diag2} \times \text{tree}_t \Rightarrow B_A(t,s), \\ &\text{diag3} \times \text{tree}_s \Rightarrow B_C(u,t), && \text{diag3} \times \text{tree}_t \Rightarrow -B_B(u,t), \\ &\text{diag4} \times \text{tree}_s \Rightarrow -B_B(u,s), && \text{diag4} \times \text{tree}_t \Rightarrow B_C(u,s).\end{aligned} \tag{68}$$

We evaluate the three form factors B_i using dispersion relations and computing thereby the convolution of the hadronic or fermionic cross-section ratio R with three kernel functions K_i,

$$B_i(x,y) = \int_{4M^2}^{\infty} dz\,\frac{R(z)}{z}K_i(x,y;z), \tag{69}$$

where R has been introduced in Eq. (31), and the kernel function are to be calculated. For positive x or y, one has to replace $x \to x + i\delta$ or $y \to y + i\delta$.

The self-energy insertion is represented by a dispersion relation, thus replacing the one-loop photon propagator by a massive effective propagator as in Eq. (29). This procedure reduces the evaluation of the two-loop diagrams to one-loop complexity with a subsequent dispersion integration. Employing standard techniques, together with the Mathematica packages AMBRE [140] and MB [141], for a reduction of one-loop integrals to scalar master integrals, the kernel functions have been finally expressed by eight one-loop master integrals $M^{(j)}(x, y; z)$,

$$K_i(x, y; z) = F_\epsilon \sum_{j=1}^{8} C_i^{(j)}(x, y; z) M^{(j)}(x, y; z), \tag{70}$$

where F_ϵ is the usual normalization factor of Eq. (26), and $C_i^{(j)}$ are rational functions of the kinematic invariants, of the space-time dimension d, and of the two masses m_e, z. The master integrals $M^{(j)}$ are shown in Fig. 8 and analytical expressions for them can be found in Appendix B. Because of their length, we do not reproduce here the explicit (exact in m_e and d dimensions) right-hand side of (70), but refer for them to the Mathematica file at the webpage [120].

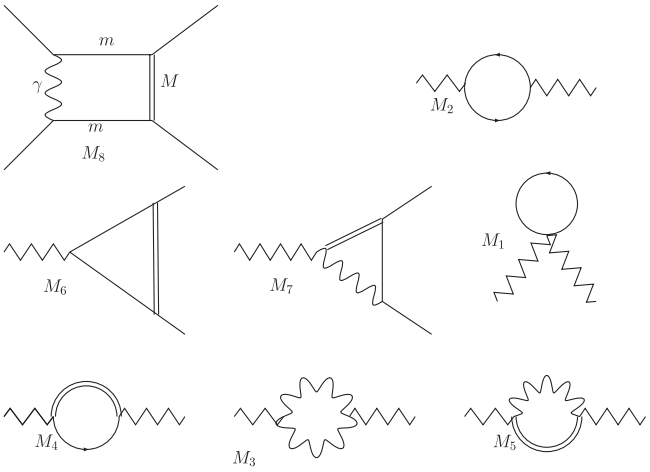

FIG. 8. The one-loop master integrals with an additional mass scale $M = \sqrt{z}$ for the dispersive two-loop box evaluation.

In the small electron-mass limit we obtain the two-loop box kernel functions:

$$\begin{aligned}
K_A(x, y; z) = \frac{1}{3(y - z)} \Bigg\{ & -2\frac{F_\epsilon}{\epsilon}(x + y)^2 \ln\left(-\frac{m_e^2}{x}\right) + 4\zeta_2\left[z^2 - z\left(\frac{x^2}{y} + y\right) + 2x(x + y) + y^2\right] \\
& + 2[z(x + y) + x^2]\ln\left(-\frac{m_e^2}{x}\right) + [z^2 + 2zx - y(2x + y)]\ln^2\left(-\frac{m_e^2}{x}\right) \\
& + \left[2z^2\left(\frac{x}{y} + 1\right) - z\left(\frac{x^2}{y} + 6x + 5y\right) + x(x + 4y) + 3y^2\right]\ln\left(-\frac{m_e^2}{y}\right) \\
& + \left[z^2 - 2z\left(\frac{x^2}{y} + x + y\right) + 2x(x + y) + y^2\right]\ln^2\left(-\frac{m_e^2}{y}\right) - 2[z^2 + 2zx + 2x(x + y) + y^2]\ln\left(-\frac{m_e^2}{x}\right) \\
& \times \ln\left(-\frac{m_e^2}{y}\right) + \left[2z^2\left(\frac{x}{y} + 1\right) - z\left(\frac{x^2}{y} + 4x + 3y\right) + (x + y)^2\right]\ln\left(\frac{z}{m_e^2}\right) + \left[2z\left(\frac{x^2}{y} + 2x + y\right) - (x + y)^2\right] \\
& \times \ln^2\left(\frac{z}{m_e^2}\right) - 2(x + y)^2 \ln\left(\frac{z}{m_e^2}\right)\ln\left(-\frac{m_e^2}{x}\right) + 2\left[z^2 - 2z\left(\frac{x^2}{y} + x + y\right) + 2x(x + y) + y^2\right]\ln\left(\frac{z}{m_e^2}\right)\ln\left(1 - \frac{z}{y}\right) \\
& - \left[2z^2\left(\frac{x}{y} + 1\right) - z\left(\frac{x^2}{y} + 6x + 5y\right) - \frac{y}{z}(x + y)^2 + 2x(x + 3y) + 4y^2\right]\ln\left(1 - \frac{z}{y}\right) \\
& + 2[z^2 + 2zx + 2x(x + y) + y^2]\ln\left(1 - \frac{z}{y}\right)\ln\left(-\frac{m_e^2}{x}\right) + 4\left[\frac{z^2}{2} - z\left(\frac{x^2}{y} + x + y\right) + x(x + y) + \frac{y^2}{2}\right]\mathrm{Li}_2\left(\frac{z}{y}\right) \\
& + 2(x + z)^2 \mathrm{Li}_2\left(1 + \frac{z}{x}\right)\Bigg\},
\end{aligned} \tag{71}$$

$$
\begin{aligned}
K_B(x,y;z) = \frac{1}{3(y-z)}\Bigg\{ & -4\frac{F_\epsilon}{\epsilon}\left[x(x+y)+\frac{y^2}{2}\right]\ln\left(-\frac{m_e^2}{x}\right) + 4\zeta_2\left[z^2 - 2z\left(\frac{x^2}{y}+\frac{y}{2}\right) + 2x(2x+y) + y^2\right] \\
& + 2[z(x+y)-xy]\ln\left(-\frac{m_e^2}{x}\right) + [z^2+2zx-y(2x+y)]\ln^2\left(-\frac{m_e^2}{x}\right) \\
& + \left[2z^2\left(\frac{x}{y}+1\right) - z\left(2\frac{x^2}{y}+6x+5y\right) + y(4x+3y) + 2x^2\right]\ln\left(-\frac{m_e^2}{y}\right) \\
& + \left[z^2 - 2z\left(2\frac{x^2}{y}+x+y\right) + 2x(2x+y)+y^2\right]\ln^2\left(-\frac{m_e^2}{y}\right) - 2[z^2+2zx+2x(2x+y)+y^2] \\
& \times \ln\left(-\frac{m_e^2}{x}\right)\ln\left(-\frac{m_e^2}{y}\right) + \left[2z^2\left(\frac{x}{y}+1\right) - z\left(2\frac{x^2}{y}+4x+3y\right) + 2x(x+y)+y^2\right]\ln\left(\frac{z}{m_e^2}\right) \\
& + 4\left[z\left(\frac{x^2}{y}+x+\frac{y}{2}\right) - \frac{x}{2}(x+y) - \frac{y^2}{4}\right]\ln^2\left(\frac{z}{m_e^2}\right) - 4\left[x(x+y)+\frac{y^2}{2}\right]\ln\left(\frac{z}{m_e^2}\right)\ln\left(-\frac{m_e^2}{x}\right) \\
& + 2\left[z^2 - 4z\left(\frac{x^2}{y}+\frac{x}{2}+\frac{y}{2}\right) + 2x(2x+y)+y^2\right]\ln\left(\frac{z}{m_e^2}\right)\ln\left(1-\frac{z}{y}\right) \\
& - \left[2z^2\left(\frac{x}{y}+1\right) - 2z\left(\frac{x^2}{y}+3x+\frac{5}{2}y\right) - 2\frac{y}{z}\left(x^2+xy+\frac{y^2}{2}\right) + 2(2x^2+2y^2+3xy)\right]\ln\left(1-\frac{z}{y}\right) \\
& + 2[z^2+2zx+2x(2x+y)+y^2]\ln\left(1-\frac{z}{y}\right)\ln\left(-\frac{m_e^2}{x}\right) + 2\left[z^2 - 2z\left(2\frac{x^2}{y}+x+y\right) + 2x(2x+y)+y^2\right] \\
& \times \mathrm{Li}_2\left(\frac{z}{y}\right) + 2(z^2+2xz+2x^2)\mathrm{Li}_2\left(1+\frac{z}{x}\right)\Bigg\},
\end{aligned}
\tag{72}
$$

$$
\begin{aligned}
K_C(x,y;z) = \frac{1}{3(y-z)}\Bigg\{ & 2\frac{F_\epsilon}{\epsilon}x^2\ln\left(-\frac{m_e^2}{x}\right) + 4\zeta_2 x^2\left(\frac{z}{y}-2\right) - 2(x^2+y^2+xy)\ln\left(-\frac{m_e^2}{x}\right) + x^2\left(\frac{z}{y}-1\right)\ln\left(-\frac{m_e^2}{y}\right) \\
& + 2x^2\left(\frac{z}{y}-1\right)\ln^2\left(-\frac{m_e^2}{y}\right) + 4x^2\ln\left(-\frac{m_e^2}{x}\right)\ln\left(-\frac{m_e^2}{y}\right) + x^2\left(\frac{z}{y}-1\right)\ln\left(\frac{z}{m_e^2}\right) - 2x^2\left(\frac{z}{y}-\frac{1}{2}\right)\ln^2\left(\frac{z}{m_e^2}\right) \\
& + 4x^2\left(\frac{z}{y}-1\right)\ln\left(\frac{z}{m_e^2}\right)\ln\left(1-\frac{z}{y}\right) + 2x^2\ln\left(\frac{z}{m_e^2}\right)\ln\left(-\frac{m_e^2}{x}\right) - x^2\left(\frac{z}{y}+\frac{y}{z}-2\right)\ln\left(1-\frac{z}{y}\right) \\
& - 4x^2\ln\left(1-\frac{z}{y}\right)\ln\left(-\frac{m_e^2}{x}\right) + 4x^2\left(\frac{z}{y}-1\right)\mathrm{Li}_2\left(\frac{z}{y}\right) - 2x^2\mathrm{Li}_2\left(1+\frac{z}{x}\right)\Bigg\}.
\end{aligned}
\tag{73}
$$

These kernel functions are reproduced in Mathematica files at the webpage [120] as functions KA, KB, KC and KA exp, KB exp, KC exp.

The two-loop box kernel masters (71) to (73) are evaluated in the Feynman gauge; they are infrared divergent and contain collinear singularities in m_e.

After inserting Eq. (71)–(73) in Eq. (69), we derive the total contribution to the cross section generated by box diagrams. Collecting powers of α, we write

$$
\begin{aligned}
\frac{d\bar{\sigma}_{\mathrm{box}}}{d\Omega} = & \int_{4M^2}^{\infty} dz \frac{R(z)}{z}\frac{1}{t-z}I_1(z) + \mathrm{Re}\int_{4M^2}^{\infty} dz \frac{R(z)}{z}\frac{1}{s-z+i\delta}\left[I_2(z) + I_3(z)\ln\left(1-\frac{z}{s+i\delta}\right)\right] \\
& + \pi\mathrm{Im}\int_{4M^2}^{\infty} dz \frac{R(z)}{z}\frac{1}{s-z+i\delta}I_3(z),
\end{aligned}
\tag{74}
$$

where the integrand functions are given by

$$I_1(z) = \frac{1}{3}\Big\{-\Big[\frac{F_\epsilon}{\epsilon} - \ln\Big(\frac{s}{m_e^2}\Big) + \ln\Big(\frac{z}{s}\Big)\Big]\ln\Big(-\frac{u}{s}\Big)\Big[\frac{v_1(t,s)}{t} + \frac{v_2(s,t)}{s}\Big] - \zeta_2\Big[2\frac{z^2}{t} - 4z\Big(1+\frac{s}{t}\Big) - \frac{t^2}{s} - 2\frac{s^2}{t} + s - t\Big]$$
$$- \Big[z\frac{s}{t} - \frac{t^2}{s} - 2(s+t)\Big]\ln\Big(1+\frac{t}{s}\Big) - \frac{1}{2}\Big[\frac{z^2}{t} - 2z\Big(1+\frac{s}{t}\Big) + 2s + t\Big]\ln^2\Big(1+\frac{t}{s}\Big)$$
$$+ \Big[z^2\Big(\frac{1}{s} + 2\frac{s}{t^2} + \frac{2}{t}\Big) - z\Big(\frac{t}{s} + 2\frac{s}{t} + 2\Big)\Big]\ln\Big(\frac{z}{s}\Big) - \Big[z^2\Big(\frac{1}{s} + \frac{1}{t}\Big) + 2z\Big(1+\frac{s}{t}\Big) + s + 2\frac{s^2}{t}\Big]\ln\Big(\frac{z}{s}\Big)\ln\Big(1+\frac{z}{s}\Big)$$
$$+ \Big[\frac{z^2}{s} + 4z\Big(1+\frac{s}{t}\Big) - \frac{t^2}{s} - 4(s+t)\Big]\Big[\ln\Big(\frac{z}{s}\Big)\ln\Big(1-\frac{z}{t}\Big) + \frac{1}{2}\ln^2\Big(-\frac{t}{s}\Big)\Big]$$
$$- \Big[z^2\Big(\frac{1}{s} + 2\frac{s}{t^2} + \frac{2}{t}\Big) - 2z\Big(\frac{t}{s} + 2\frac{s}{t} + 2\Big) + \frac{t^2}{s} + 2(s+t)\Big]\Big[\ln\Big(1-\frac{z}{t}\Big) + \ln\Big(-\frac{t}{s}\Big)\Big]$$
$$+ \Big[\frac{z^2}{t} - 2z\Big(1+\frac{s}{t}\Big) + 2\frac{t^2}{s} + 8s + 4\frac{s^2}{t} + 7t\Big]\Big[\ln\Big(1-\frac{z}{t}\Big) + \ln\Big(-\frac{t}{s}\Big)\Big]\ln\Big(1+\frac{t}{s}\Big)$$
$$- \Big[z^2\Big(\frac{1}{s} + \frac{1}{t}\Big) + 2z\Big(1+\frac{s}{t}\Big) + s + 2\frac{s^2}{t}\Big]\mathrm{Li}_2\Big(-\frac{z}{s}\Big) + \Big[\frac{z^2}{s} + 4z\Big(1+\frac{s}{t}\Big) - \frac{t^2}{s} - 4(s+t)\Big]\mathrm{Li}_2\Big(\frac{z}{t}\Big)$$
$$- \Big[\frac{z^2}{t} - 2z\Big(1+\frac{s}{t}\Big) + \frac{t^2}{s} + 5s + 2\frac{s^2}{t} + 4t\Big]\mathrm{Li}_2\Big(1+\frac{z}{u}\Big)\Big\}, \tag{75}$$

$$I_2(z) = \frac{1}{3}\Big\{-\Big[\frac{F_\epsilon}{\epsilon} - \ln\Big(\frac{s}{m_e^2}\Big) + \ln\Big(\frac{z}{s}\Big)\Big]\ln\Big(\frac{u}{t}\Big)\Big[\frac{v_1(s,t)}{s} + \frac{v_2(s,t)}{t}\Big] - \Big[z\frac{t}{s} - \frac{s^2}{t} - 2(s+t)\Big]\ln\Big(1+\frac{t}{s}\Big)$$
$$- \frac{1}{2}\Big[\frac{z^2}{s} - 2z\Big(1+\frac{t}{s}\Big) + s + 2t\Big]\ln^2\Big(1+\frac{t}{s}\Big) - z\Big(\frac{t}{s} + \frac{s}{t} + 2\Big)\ln\Big(-\frac{t}{s}\Big)$$
$$+ \frac{1}{2}\Big[z^2\Big(\frac{1}{s} + \frac{1}{t}\Big) + 2z\Big(1+\frac{t}{s}\Big) - \frac{s^2}{t} - 3s - 2t\Big]\ln^2\Big(-\frac{t}{s}\Big) + \Big[z^2\Big(\frac{1}{t} + \frac{2}{s} + 2\frac{t}{s^2}\Big) - z\Big(\frac{s}{t} + 2 + 2\frac{t}{s}\Big)\Big]\ln\Big(\frac{z}{s}\Big)$$
$$- \Big[\frac{z^2}{t} + 4z\Big(1+\frac{t}{s}\Big) - \frac{s^2}{t} - 4(s+t)\Big]\mathrm{Li}_2\Big(1-\frac{z}{s}\Big) + \Big[z^2\Big(\frac{1}{s} + \frac{1}{t}\Big) + 2z\Big(1+\frac{t}{s}\Big) + 2\frac{t^2}{s} + t\Big]\mathrm{Li}_2\Big(1+\frac{z}{t}\Big)$$
$$- \Big[\frac{z^2}{s} - 2z\Big(1+\frac{t}{s}\Big) + \frac{s^2}{t} + 2\frac{t^2}{s} + 4s + 5t\Big]\mathrm{Li}_2\Big(1+\frac{z}{u}\Big)\Big\}, \tag{76}$$

$$I_3(z) = \frac{1}{3}\Big\{\Big[\frac{z^2}{s} - 2z\Big(1+\frac{t}{s}\Big) + 4\frac{t^2}{s} + 2\frac{s^2}{t} + 7s + 8t\Big]\ln\Big(1+\frac{t}{s}\Big) - \Big[z^2\Big(\frac{1}{s} + \frac{1}{t}\Big) + 2z\Big(1+\frac{t}{s}\Big) + 4\frac{t^2}{s} + \frac{s^2}{t} + 3s + 4t\Big]$$
$$\times \ln\Big(-\frac{t}{s}\Big) - \Big[z^2\Big(\frac{1}{t} + \frac{2}{s} + 2\frac{t}{s^2}\Big) - 2z\Big(2 + \frac{s}{t} + 2\frac{t}{s}\Big) + \frac{s^2}{t} + 2(s+t)\Big]\Big\}. \tag{77}$$

The functions $I_1(z)$ to $I_3(z)$ are reproduced as functions I_1, I_2, I_3 in a Mathematica file at the webpage [120].

Note that, after assembling all irreducible box diagrams, their total contribution is free of collinear divergencies in m_e because $\ln(m_e^2)$ vanishes in the combination

$$\frac{F_\epsilon}{\epsilon} - \ln\Big(\frac{s}{m_e^2}\Big) = \frac{1}{\epsilon} - \gamma_E - \ln(\pi) - \ln\Big(\frac{s}{\mu^2}\Big) + 0(\epsilon). \tag{78}$$

This fact might be observed already for any sum of single pairs of direct and their related crossed box diagrams, which is gauge-independent and free of collinear singularities [142]; from (68) and Fig. 7 one selects e.g. the following ones:

$$K_B(t,s;z) - K_B(u,s;z), \qquad K_A(s,t;z) + K_C(u,t;z). \tag{79}$$

In the limit $m_f^2 \ll s, |t|, |u|$, the z-integration over the $I_i(z)$, $i = 1, 2$, develops mass singularities from the lower integration bound:

$$\int_{4M^2}^{\infty} dz \frac{R(z)}{z} K_{\mathrm{SE}}(y;z)\Big[A(x,y,z) + B(x,y)\ln\Big(\frac{z}{s}\Big)\Big] \tag{80}$$

where A, B are regular for $z \to 0$. It follows immediately that the irreducible box diagrams yield terms of the order of at most $\ln^2(s/m_f^2)$, because A joins, after integration, terms with a behavior like a one-loop self-energy, and B joins terms with one order more in the logarithmic structure. This has been discussed already in [113].

The residual infrared-singular part of the box cross section is:

$$\frac{d\bar{\sigma}^{\mathrm{IR}}_{\mathrm{box}}}{d\Omega} = -\left[\frac{F_\epsilon}{\epsilon} - \ln(\hat{s})\right]\left\{\ln\left(-\frac{u}{s}\right)\left[\frac{v_1(t,s)}{t^2} + \frac{v_2(s,t)}{st}\right]I(t) + \ln\left(\frac{u}{t}\right)\left[\frac{v_1(s,t)}{s^2} + \frac{v_2(s,t)}{st}\right]I(s)\right\}. \quad (81)$$

The function $I(t)$ [see Eq. (57)] stems from diagrams with a vacuum-polarization insertion in the t-channel, and $I(s)$ from insertions in the s-channel. One may wonder which of the other infrared divergent parts are needed to compensate the double-box divergency (in the gauge chosen here). This may be exemplified by collecting all the IR-divergencies of the diagrams with a vacuum polarization insertion $I(t)$ in the t-channel; for the others, quite analogous arguments hold. From Secs. VI A and VI B we may extract such terms. There are the following divergencies due to vertex diagrams:

$$\frac{d\bar{\sigma}^{a,\mathrm{IR}}_{\mathrm{fact}}}{d\Omega} = \left[\frac{F_\epsilon}{\epsilon} - \ln(\hat{s})\right]\left[\ln(\hat{s}) - 1 + \ln\left(-\frac{t}{s}\right)\right] \times \left(\frac{v_1}{t^2} + \frac{v_2}{st}\right)I(t), \quad (82)$$

$$\frac{d\bar{\sigma}^{b,\mathrm{IR}}_{\mathrm{fact}}}{d\Omega} = \left[\frac{F_\epsilon}{\epsilon} - \ln(\hat{s})\right]\left\{\left[\ln(\hat{s}) - 1 + \ln\left(-\frac{t}{s}\right)\right]\frac{v_1}{t^2} + [\ln(\hat{s}) - 1]\frac{v_2}{st}\right\}I(t). \quad (83)$$

The reducible box diagrams are (in the curly brackets) free of electron mass singularities, also in the terms not shown here. They depend also on u:

$$\frac{d\bar{\sigma}^{c,\mathrm{IR}}_{\mathrm{fact}}}{d\Omega} = \left[\frac{F_\epsilon}{\epsilon} - \ln(\hat{s})\right]\left\{\left[-\ln\left(-\frac{u}{s}\right)\right]\frac{v_1}{t^2} + \left[-\ln\left(-\frac{u}{s}\right) - \ln\left(-\frac{t}{s}\right)\right]\frac{v_2}{st}\right\}I(t). \quad (84)$$

For the soft real terms, we refer to Appendix C and may distinguish between initial and final state corrections (which are equal) and the initial-final state interference:

$$\frac{d\bar{\sigma}^{d,\mathrm{int,IR}}_{\mathrm{fact}}}{d\Omega} = \left[\frac{F_\epsilon}{\epsilon} - \ln(\hat{s})\right]\left[2\ln\left(-\frac{u}{s}\right) - 2\ln\left(-\frac{t}{s}\right)\right] \times \left(\frac{v_1}{t^2} + \frac{v_2}{st}\right)I(t), \quad (85)$$

$$\frac{d\bar{\sigma}^{d,\mathrm{ini+fin,IR}}_{\mathrm{fact}}}{d\Omega} = \left[\frac{F_\epsilon}{\epsilon} - \ln(\hat{s})\right][-2\ln(\hat{s}) + 2]\left(\frac{v_1}{t^2} + \frac{v_2}{st}\right)I(t). \quad (86)$$

It is now easy to see that the IR-divergency of the double box diagrams, being proportional to $\ln(-u/s)$, gets completely canceled by the sum of the reducible box diagrams and the interference part of soft bremsstrahlung. Although, the latter introduce to the sum an IR-divergency with $\ln(-t/s)$, and this gets canceled the reducible vertex diagrams, thus introducing an IR-divergency with $\ln(s/m_e^2)$, which will be canceled finally by the initial and final state soft corrections. The lesson is: a sensible, infrared safe cross section contains the complete sum of all the single IR-divergent diagrams, or no one of them.

Despite that, an isolated treatment of the pure self energies or of the irreducible vertex corrections is possible.

Finally, we just mention that the analytical integrations over z may be performed following the hints in Sec. V.

D. Kernel functions for the infrared safe sum

We are now in a state to evaluate the net cross-section contribution from the various infrared divergent terms of Secs. VI A and VI C. We have seen that they have to be treated together. The sum of the box contributions of Eq. (74) with all infrared-divergent factorizable corrections, given in Eqs. (58) and (60)–(62), is infrared-finite and can be cast in the following form:

$$\frac{d\bar{\sigma}_{\mathrm{rest}}}{d\Omega} = \frac{d\bar{\sigma}_{\mathrm{box}}}{d\Omega} + \sum_{i=a,b,c,d}\frac{d\bar{\sigma}^i_{\mathrm{fact}}}{d\Omega} = \int_{4M^2}^{\infty} dz \frac{R(z)}{z}\frac{1}{t-z}F_1(z) + \mathrm{Re}\int_{4M^2}^{\infty} dz \frac{R(z)}{z}\frac{1}{s-z+i\delta}\left[F_2(z) + F_3(z)\ln\left(1 - \frac{z}{s+i\delta}\right)\right] + \pi\mathrm{Im}\int_{4M^2}^{\infty} dz \frac{R(z)}{z}\frac{1}{s-z+i\delta}F_4(z). \quad (87)$$

The lower bound is $4M^2 = 4m_\pi^2$ for hadrons and $4M^2 = 4m_f^2$ for fermions f. The auxiliary functions $F_i(z)$ are given by

$$
\begin{aligned}
F_1(z) = \frac{1}{3}\Bigg\{&\Bigg[3\Big(\frac{t^2}{s}+2\frac{s^2}{t}\Big)+9(s+t)\Bigg]\ln\Big(\frac{s}{m_e^2}\Big)+\Bigg[-z^2\Big(\frac{1}{s}+\frac{2}{t}+2\frac{s}{t^2}\Big)+z\Big(4+4\frac{s}{t}+2\frac{t}{s}\Big)+\frac{1}{2}\frac{t^2}{s}+6\frac{s^2}{t}+5s+4t\Bigg]\\
&\times\ln\Big(-\frac{t}{s}\Big)+s\Big(-\frac{z}{t}+\frac{3}{2}\Big)\ln\Big(1+\frac{t}{s}\Big)+\Bigg[\frac{1}{2}\frac{z^2}{s}+2z\Big(1+\frac{s}{t}\Big)-\frac{11}{4}s-2t\Bigg]\ln^2\Big(-\frac{t}{s}\Big)\\
&-\Bigg[\frac{1}{2}\frac{z^2}{t}-z\Big(1+\frac{s}{t}\Big)+\frac{t^2}{s}+2\frac{s^2}{t}+\frac{9}{2}s+\frac{15}{4}t\Bigg]\ln^2\Big(1+\frac{t}{s}\Big)+\Bigg[\frac{z^2}{t}-2z\Big(1+\frac{s}{t}\Big)+2\frac{s^2}{t}+5s+\frac{5}{2}t\Bigg]\ln\Big(-\frac{t}{s}\Big)\\
&\times\ln\Big(1+\frac{t}{s}\Big)-4\Bigg[\frac{t^2}{s}+2\frac{s^2}{t}+3(s+t)\Bigg]\Bigg[1+\mathrm{Li}_2\Big(-\frac{t}{s}\Big)\Bigg]-\Bigg[2\frac{z^2}{t}-4z\Big(1+\frac{s}{t}\Big)-4\frac{t^2}{s}-2\frac{s^2}{t}+s-\frac{11}{2}t\Bigg]\zeta_2\\
&-\Bigg[\frac{t^2}{s}+2\frac{s^2}{t}+3(s+t)\Bigg]\ln\Big(\frac{z}{s}\Big)\ln\Big(1+\frac{t}{s}\Big)+\Bigg[z^2\Big(\frac{1}{s}+2\frac{s}{t^2}+\frac{2}{t}\Big)-z\Big(\frac{t}{s}+2\frac{s}{t}+2\Big)\Bigg]\ln\Big(\frac{z}{s}\Big)\\
&-\Bigg[z^2\Big(\frac{1}{s}+\frac{1}{t}\Big)+2z\Big(1+\frac{s}{t}\Big)+s+2\frac{s^2}{t}\Bigg]\ln\Big(\frac{z}{s}\Big)\ln\Big(1+\frac{z}{s}\Big)+\Bigg[\frac{z^2}{s}+4z\Big(1+\frac{s}{t}\Big)-\frac{t^2}{s}-4(s+t)\Bigg]\ln\Big(\frac{z}{s}\Big)\ln\Big(1-\frac{z}{t}\Big)\\
&-\Bigg[z^2\Big(\frac{1}{s}+2\frac{s}{t^2}+\frac{2}{t}\Big)-2z\Big(\frac{t}{s}+2\frac{s}{t}+2\Big)+\frac{t^2}{s}+2(s+t)\Bigg]\ln\Big(1-\frac{z}{t}\Big)\\
&+\Bigg[\frac{z^2}{t}-2z\Big(1+\frac{s}{t}\Big)+2\frac{t^2}{s}+8s+4\frac{s^2}{t}+7t\Bigg]\ln\Big(1-\frac{z}{t}\Big)\ln\Big(1+\frac{t}{s}\Big)-\Bigg[z^2\Big(\frac{1}{s}+\frac{1}{t}\Big)+2z\Big(1+\frac{s}{t}\Big)+s+2\frac{s^2}{t}\Bigg]\\
&\times\mathrm{Li}_2\Big(-\frac{z}{s}\Big)+\Bigg[\frac{z^2}{s}+4z\Big(1+\frac{s}{t}\Big)-\frac{t^2}{s}-4(s+t)\Bigg]\mathrm{Li}_2\Big(\frac{z}{t}\Big)-\Bigg[\frac{z^2}{t}-2z\Big(1+\frac{s}{t}\Big)+\frac{t^2}{s}+5s+2\frac{s^2}{t}+4t\Bigg]\mathrm{Li}_2\Big(1+\frac{z}{u}\Big)\Bigg\}\\
&+4\Big(\frac{1}{3}\frac{t^2}{s}+\frac{2}{3}\frac{s^2}{t}+s+t\Big)\ln\Big(\frac{2\omega}{\sqrt{s}}\Big)\Bigg[\ln\Big(\frac{s}{m_e^2}\Big)+\ln\Big(-\frac{t}{s}\Big)-\ln\Big(1+\frac{t}{s}\Big)-1\Bigg],
\end{aligned}
\tag{88}
$$

$$
\begin{aligned}
F_2(z) = \frac{1}{3}\Bigg\{&\Bigg[6\frac{t^2}{s}+3\frac{s^2}{t}+9(s+t)\Bigg]\ln\Big(\frac{s}{m_e^2}\Big)-\Bigg[z\Big(\frac{t}{s}+\frac{s}{t}+2\Big)-5\Big(s+\frac{t}{2}+\frac{1}{2}\frac{s^2}{t}\Big)\Bigg]\ln\Big(-\frac{t}{s}\Big)-t\Big(\frac{z}{s}-\frac{3}{2}\Big)\ln\Big(1+\frac{t}{s}\Big)\\
&+\Bigg[\frac{z^2}{2}\Big(\frac{1}{s}+\frac{1}{t}\Big)+z\Big(1+\frac{t}{s}\Big)+2\frac{t^2}{s}-\frac{s}{4}+\frac{3}{4}t\Bigg]\ln^2\Big(-\frac{t}{s}\Big)-\Bigg[\frac{z^2}{2s}-z\Big(1+\frac{t}{s}\Big)+2\frac{t^2}{s}+\frac{s^2}{t}+\frac{15}{4}s+\frac{9}{2}t\Bigg]\ln^2\Big(1+\frac{t}{s}\Big)\\
&-\Big(4\frac{t^2}{s}+\frac{s^2}{t}+4s+5t\Big)\ln\Big(-\frac{t}{s}\Big)\ln\Big(1+\frac{t}{s}\Big)-4\Bigg[2\frac{t^2}{s}+\frac{s^2}{t}+3(s+t)\Bigg]\Bigg[1+\mathrm{Li}_2\Big(-\frac{t}{s}\Big)\Bigg]\\
&+\Big(12\frac{t^2}{s}+3\frac{s^2}{t}+12s+15t\Big)\zeta_2-\Bigg[2\frac{t^2}{s}+\frac{s^2}{t}+3(s+t)\Bigg]\ln\Big(\frac{z}{s}\Big)\Bigg[\ln\Big(1+\frac{t}{s}\Big)-\ln\Big(-\frac{t}{s}\Big)\Bigg]\\
&+\Bigg[z^2\Big(\frac{1}{t}+\frac{2}{s}+2\frac{t}{s^2}\Big)-z\Big(\frac{s}{t}+2+2\frac{t}{s}\Big)\Bigg]\ln\Big(\frac{z}{s}\Big)-\Bigg[\frac{z^2}{t}+4z\Big(1+\frac{t}{s}\Big)-\frac{s^2}{t}-4(s+t)\Bigg]\mathrm{Li}_2\Big(1-\frac{z}{s}\Big)\\
&+\Bigg[z^2\Big(\frac{1}{s}+\frac{1}{t}\Big)+2z\Big(1+\frac{t}{s}\Big)+2\frac{t^2}{s}+t\Bigg]\mathrm{Li}_2\Big(1+\frac{z}{t}\Big)-\Bigg[\frac{z^2}{s}-2z\Big(1+\frac{t}{s}\Big)+\frac{s^2}{t}+2\frac{t^2}{s}+4s+5t\Bigg]\mathrm{Li}_2\Big(1+\frac{z}{u}\Big)\Bigg\}\\
&+4\Big(\frac{2}{3}\frac{t^2}{s}+\frac{1}{3}\frac{s^2}{t}+s+t\Big)\ln\Big(\frac{2\omega}{\sqrt{s}}\Big)\Bigg[\ln\Big(\frac{s}{m_e^2}\Big)+\ln\Big(-\frac{t}{s}\Big)-\ln\Big(1+\frac{t}{s}\Big)-1\Bigg],
\end{aligned}
\tag{89}
$$

$$
F_3(z) = I_3(z), \tag{90}
$$

$$
\begin{aligned}
F_4(z) = \frac{1}{3}\Bigg\{&\Bigg[\frac{z^2}{s}-2z\Big(1+\frac{t}{s}\Big)+2\frac{t^2}{s}+2\frac{s^2}{t}+\frac{11}{2}s+5t\Bigg]\ln\Big(1+\frac{t}{s}\Big)-\Bigg[z^2\Big(\frac{1}{s}+\frac{1}{t}\Big)+2z\Big(1+\frac{t}{s}\Big)+2\frac{t^2}{s}+\frac{3}{2}s+\frac{5}{2}t\Bigg]\\
&\times\ln\Big(-\frac{t}{s}\Big)-\Bigg[z^2\Big(\frac{1}{t}+\frac{2}{s}+2\frac{t}{s^2}\Big)-2z\Big(2+\frac{s}{t}+2\frac{t}{s}\Big)-\frac{1}{2}\frac{s^2}{t}-s\Bigg]\Bigg\}.
\end{aligned}
\tag{91}
$$

The $I_3(z)$ is defined in (77). For $0 < s < 4M^2$ we can write

$$\frac{d\bar{\sigma}_{\text{rest}}}{d\Omega} = \int_{4M^2}^{\infty} dz \frac{R(z)}{z}\left\{\frac{1}{t-z}F_1(z) + \frac{1}{s-z}\left[F_2(z) + F_3(z)\ln\left(\frac{z}{s}-1\right)\right]\right\}. \quad (92)$$

For $s > 4M^2$, we have to perform some subtractions in order to make the formulas explicitly stable around $z = s$, and at the time retain the sufficiently fast vanishing of the integrand at $z \to \infty$:

$$\begin{aligned}\frac{d\bar{\sigma}_{\text{rest}}}{d\Omega} = &\int_{4M^2}^{\infty} dz \frac{R(z)}{z}\frac{1}{t-z}F_1(z) \\ &+ \int_{4M^2}^{\infty} dz \frac{1}{z(s-z)}\Big\{R(z)F_2(z) - R(s)F_2(s) \\ &+ [R(z)F_3(z) - R(s)F_3(s)]\ln\left|1-\frac{z}{s}\right|\Big\} \\ &+ \frac{R(s)}{s}\Big\{F_2(s)\ln\left(\frac{s}{4M^2}-1\right) - 6\zeta_2 F_4(s) \\ &+ F_3(s)\Big[2\zeta_2 + \frac{1}{2}\ln^2\left(\frac{s}{4M^2}-1\right) \\ &+ \mathrm{Li}_2\left(1-\frac{s}{4M^2}\right)\Big]\Big\}. \quad (93)\end{aligned}$$

In the limit $m_f^2 \ll s$, $|t|$, $|u|$, the z-integration over the $F_i(z)$, $i = 1, 2$, develops mass singularities from the lower integration bound:

$$\int_{4M^2} dz \frac{R(z)}{z} K_{\text{SE}}(y; z)\Big[A(x, y, z) + B(x, y)\ln\left(\frac{z}{s}\right) + C(x, y)\ln\left(\frac{s}{m_e^2}\right)\Big] \quad (94)$$

where A, B, C are regular for $z \to 0$. It follows immediately that the sum of all infrared divergent diagrams yield terms of the order of at most $\ln^2(s/m_f^2)$ and $\ln(s/m_e^2)\ln(s/m_f^2)$, because A joins, after integration, terms with a behavior like a one-loop self-energy, B joins terms with one order more in $\ln(s/m_f^2)$ and C goes together with at most $\ln(s/m_e^2)\ln(s/m_f^2)$; there are no cubic logarithms here. This has been discussed already in [113].

Further, for the numerical evaluation, the functions F_1, F_2, and F_3 are replaced for $z \to \infty$ by their asymptotic values:

$$\begin{aligned}F_1(z) \sim &\left[\frac{t^2}{s} + 2\frac{s^2}{t} + 3(s+t)\right]\ln\left(\frac{s}{m_e^2}\right) + \left[\frac{1}{2}\frac{t^2}{s} + 2\frac{s^2}{t} + \frac{7}{3}s + 2t\right]\ln\left(-\frac{t}{s}\right) + \frac{s}{2}\left(\frac{1}{3} - \frac{s}{t}\right)\ln\left(1+\frac{t}{s}\right) \\ &- \frac{1}{2}\left(\frac{s}{2} - \frac{1}{3}\frac{t^2}{s}\right)\ln^2\left(-\frac{t}{s}\right) - \frac{1}{3}\left(\frac{1}{2}\frac{t^2}{s} + \frac{s^2}{t} + 2s + \frac{7}{4}t\right)\ln^2\left(1+\frac{t}{s}\right) - \left[\frac{2}{3}\left(\frac{t^2}{s} + \frac{s^2}{t}\right) + s + \frac{3}{2}t\right]\ln\left(-\frac{t}{s}\right)\ln\left(1+\frac{t}{s}\right) \\ &- 4\left[\frac{1}{3}\left(\frac{t^2}{s} + 2\frac{s^2}{t}\right) + s + t\right]\mathrm{Li}_2\left(-\frac{t}{s}\right) + \left[2\left(\frac{t^2}{s} + \frac{s^2}{t}\right) + 3\left(s + \frac{3}{2}t\right)\right]\zeta_2 - \left[\frac{23}{12}\frac{t^2}{s} + \frac{8}{3}\frac{s^2}{t} + \frac{23}{4}(s+t)\right] \\ &- \frac{1}{2}\left[\frac{t^2}{s} + 3(s+t)\right]\ln\left(\frac{z}{s}\right) + 4\left(\frac{1}{3}\frac{t^2}{s} + \frac{2}{3}\frac{s^2}{t} + s + t\right)\ln\left(\frac{2\omega}{\sqrt{s}}\right)\left[\ln\left(\frac{s}{m_e^2}\right) + \ln\left(-\frac{t}{s}\right) - \ln\left(1+\frac{t}{s}\right) - 1\right] + \mathcal{O}\left(\frac{1}{z}\right), \quad (95)\end{aligned}$$

$$F_s(z) = F_2(z) + F_3(z)\ln\left(\frac{z}{s}-1\right), \quad (96)$$

$$\begin{aligned}F_s(z) \sim &\left[2\frac{t^2}{s} + \frac{s^2}{t} + 3(s+t)\right]\ln\left(\frac{s}{m_e^2}\right) + \left(\frac{1}{2}\frac{t^2}{s} + \frac{s^2}{t} + \frac{5}{2}s + 2t\right)\ln\left(-\frac{t}{s}\right) + \frac{t}{2}\left(\frac{1}{3} - \frac{t}{s}\right)\ln\left(1+\frac{t}{s}\right) \\ &+ \frac{1}{3}\left[\frac{t^2}{s} - \frac{1}{4}(s-t)\right]\ln^2\left(-\frac{t}{s}\right) - \frac{1}{3}\left(\frac{t^2}{s} + \frac{1}{2}\frac{s^2}{t} + \frac{7}{4}s + 2t\right)\ln^2\left(1+\frac{t}{s}\right) - \frac{1}{3}\left(4\frac{t^2}{s} + \frac{s^2}{t} + 4s + 5t\right)\ln\left(-\frac{t}{s}\right)\ln\left(1+\frac{t}{s}\right) \\ &- 4\left(\frac{2}{3}\frac{t^2}{s} + \frac{1}{3}\frac{s^2}{t} + s + t\right)\mathrm{Li}_2\left(-\frac{t}{s}\right) + \left(4\frac{t^2}{s} + \frac{s^2}{t} + 4s + 5t\right)\zeta_2 - \left[\frac{8}{3}\frac{t^2}{s} + \frac{23}{12}\frac{s^2}{t} + \frac{23}{4}(s+t)\right] \\ &- \frac{1}{2}\left[\frac{s^2}{t} + 3(s+t)\right]\ln\left(\frac{z}{s}\right) + 4\left(\frac{2}{3}\frac{t^2}{s} + \frac{1}{3}\frac{s^2}{t} + s + t\right)\ln\left(\frac{2\omega}{\sqrt{s}}\right)\left[\ln\left(\frac{s}{m_e^2}\right) + \ln\left(-\frac{t}{s}\right) - \ln\left(1+\frac{t}{s}\right) - 1\right] + \mathcal{O}\left(\frac{1}{z}\right). \quad (97)\end{aligned}$$

TABLE III. Numerical values for the differential cross section in nanobarns at scattering angles $\theta = 20°$ and $\theta = 3°$, in units of 10^2. Concerning the finite remainder, containing irreducible box diagrams, we show for each fermion flavor the result obtained through the dispersion-based approach (first line) and the one coming from the analytical expansion (second line), neglecting $\mathcal{O}(m_f^2/x)$, where $x = s, |t|, |u|$. When $m_f^2 > x$, the entry is suppressed.

$\theta[°]\|\sqrt{s}$ [GeV]	$\theta = 20\|1$	$\theta = 20\|10$	$\theta = 3\|M_Z$	$\theta = 3\|500$
QED Born	214.903	2.149 03	53.0348	1.763 98
weak Born	214.903	2.149 30	53.0376	1.763 90
QED Born, running	218.559	2.238 14	55.5353	1.909 10
vertices [$\mu + \tau$ + hadr]	−0.001 086	−0.000 225 13	−0.007 982	−0.001 292 96
vertices [e]	−0.102 787	−0.003 254 49	−0.092 546	−0.005 745 77
soft pairs e^+e^-	0.130 264	0.004 037 72	0.112 763	0.006 858 90
rest: e	0.235 562	0.004 978 34	0.135 650	0.006 726 52
μ	0.009 518	0.001 350 40	0.040 792	0.002 878 09
	−0.017 214	0.001 342 82	0.040 688	0.002 877 95
τ	0.000 074	0.000 053 85	0.002 706–0.009 610	0.000 876 39
	×	×		0.000 839 69
hadr	0.008 642	0.002 694 90	0.087 618	0.008 107 81

VII. NUMERICAL RESULTS AT MESON FACTORIES, LEP/GIGAZ, ILC

We begin with numerical results for Eq. (87), multiplied by the overall factor $(\alpha/\pi)^2\,\alpha^2/s$. The expressions contain the contribution of irreducible two-loop boxes, summed up with reducible two-loop vertex and loop-by-loop diagrams, and combined with soft-photon emission. They are called here "rest" from electrons, muons, tau-leptons, and from hadrons. The top influence was also considered but comes out so marginal that we do not discuss it. The results are summarized in Tables III and IV for small- and large-angle scattering and a variety of energy scales. We do not discuss the isolated irreducible two-loop boxes because this would become more convention-dependent. Note further that in these tables the dependence on the maximal energy of the soft photons is switched off by setting $\omega = \sqrt{s}/2$ (an analogous consideration holds for the soft pairs e^+e^-). For comparison, the tables also contain entries with pure QED Born, QED Born with running coupling, and effective weak Born cross sections, as well as contributions from: electron vertex insertions and soft e^+e^- pairs (with a quite small sum of them); the sum of heavy fermion irreducible vertices. The hadronic results have been obtained using the parametrization [133] with flag setting IPAR = 0 and implementing narrow resonances as described in Appendix E.

We see that the two-loop corrections from electron insertions (the so-called $N_f = 1$ corrections) are the largest, and the second-largest ones are the hadronic corrections. The tables also demonstrate that the approximation $m_f^2 \ll s, |t|, |u|$ as applied in e.g. [113] works well in the regions where this is expected.

A more detailed picture of the relevance of the fermionic and hadronic two-loop corrections may be got from

TABLE IV. Numerical values for the differential cross section in nanobarns at a scattering angle $\theta = 90°$, in units of 10^{-4}. See the caption of Table III for further details.

$\sqrt{s}$ [GeV]	1	10	M_Z	500
QED Born	466 537	4665.37	56.1067	1.866 15
weak Born	466 526	4654.16	1238.7500	0.928 90
QED Born, running	480 106	4984.83	62.9027	2.179 57
vertices [$\mu + \tau$ + hadr]	−16.351	−2.0437	−0.125 208	−0.010 427 5
vertices [e]	−477.620	−12.3010	−0.298 589	−0.015 575 1
soft pairs e^+e^-	648.275	16.0690	0.376 531	0.019 199 0
rest: e	807.476	14.5277	0.270 575	0.011 928 5
μ	160.197	6.0819	0.147 046	0.007 257 9
	152.890	6.0809	0.147 046	0.007 257 9
τ	2.383	1.3335	0.075 268	0.004 571 3
	×	1.0739	0.075 214	0.004 571 2
hadr	232.674	16.0670	0.469 944	0.024 603 5

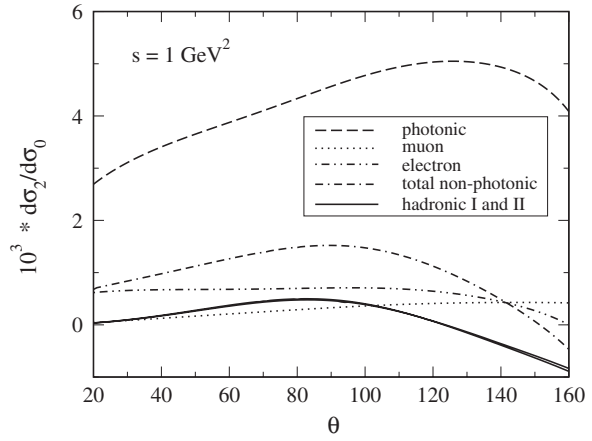

FIG. 9. Two-loop corrections to Bhabha scattering at $\sqrt{s} =$ 1 GeV, normalized to the QED tree-level cross section.

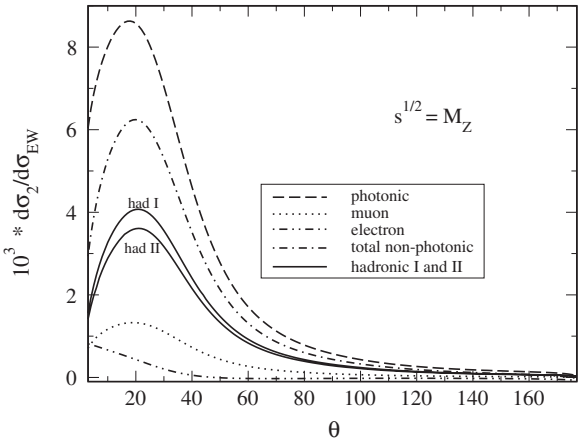

FIG. 11. Two-loop corrections to Bhabha scattering at $\sqrt{s} =$ M_Z, normalized to the effective weak Born cross section.

Figs. 9–14, where we show the cross-section ratios

$$10^3 \frac{d\sigma_{\mathrm{NNLO}}}{d\sigma_0}, \tag{98}$$

where $d\sigma_0$ is the effective weak Born cross section at $\sqrt{s} =$ M_Z, 500 and 800 GeV, and the QED Born cross section elsewhere. So, the figures show just the relative size of the corrections in per mille. For a comparison, we show also the pure photonic corrections. The $d\sigma_{\mathrm{NNLO}}$ is here the net sum of all the terms discussed arising from a fermion flavor (e or μ) or from the hadrons. In case of electrons, we add also the real pair correction. The total nonphotonic term includes also the τ and top-quark contributions. For hadrons, we decided to use the parametrization $R_{\mathrm{had,I}}$ as given in [133] with parameter IPAR = 1. We applied also numerics with a combination $R_{\mathrm{had,II}}$ of several adjusted pieces valid at different scales, as explained in Appendix E. In Figs. 9 and 11 it is seen that the predictions with $R_{\mathrm{had,I}}$ and $R_{\mathrm{had,II}}$ are quite close to each other. Because we did not get a stable numerics over all the parameter space with $R_{\mathrm{had,II}}$, we decided not to use it for the final determination of the physical results until we have a better understanding of its behavior.

We conclude this section showing a set of plots based on our work (hadronic and heavy-fermion corrections), on the photonic result obtained by A. A. Penin in [104] and on the electron-loop result of R. Bonciani *et al.* [100]. Concerning the latter case, we incorporate also the contribution of real soft electron-positron pairs with logarithmic accuracy evaluated by A. B. Arbuzov *et al.* in [44].

At a meson factory with $\sqrt{s} \approx 1$ GeV (Fig. 9) the heavy-fermion effects are below 0.5 per mille and are thus certainly negligible. At $\sqrt{s} \approx 10$ GeV (Fig. 10), electron and hadron corrections amount to 2 to 5 per mille and might play some relevance. At the higher energies, we have to consider small angles and large ones separately. The hadronic corrections amount to up to 4 per mille at LEP1/GigaZ and 20 per mille at ILC energies at large angles, while at small angles they stay well below 5 per mille. For $\sqrt{s} = 500$ GeV this is exemplified in Fig. 13, and from the tables one may read exact values at $\theta = 3$ deg: for the

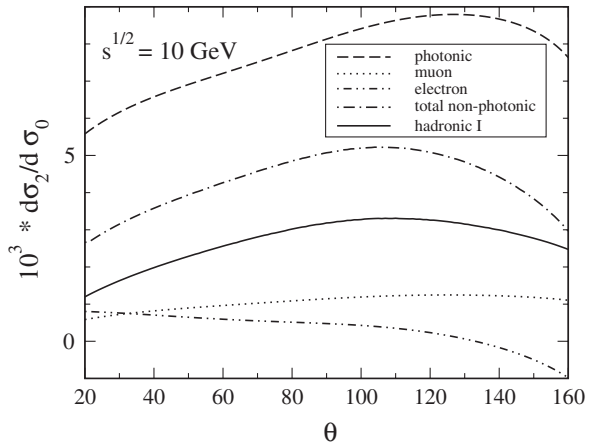

FIG. 10. Two-loop corrections to Bhabha scattering at $\sqrt{s} =$ 10 GeV, normalized to the QED tree-level cross section.

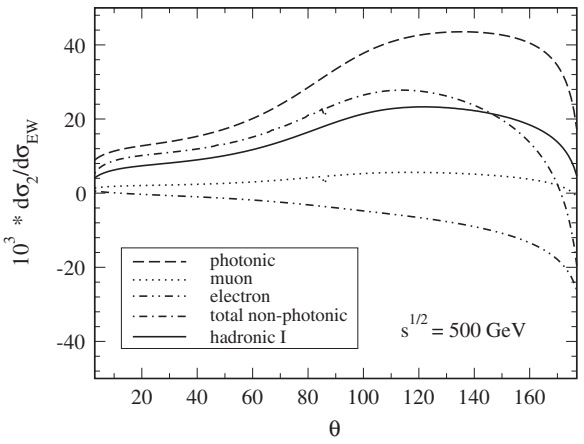

FIG. 12. Two-loop corrections to Bhabha scattering at $\sqrt{s} =$ 500 GeV, normalized to the effective weak Born cross section.

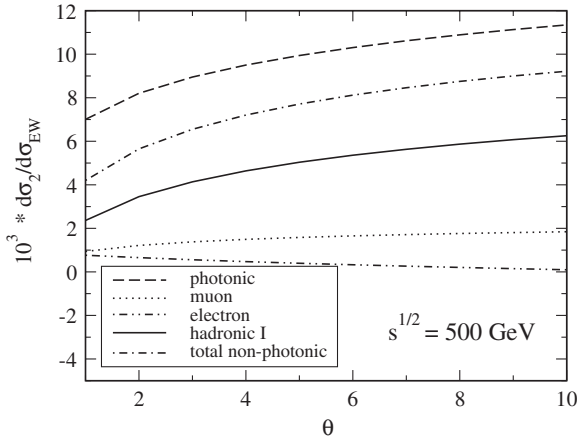

FIG. 13. Same as in Fig. 12, for small angles.

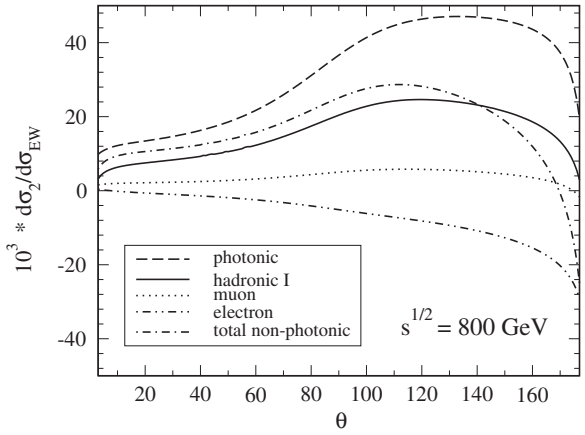

FIG. 14. Two-loop corrections to Bhabha scattering at $\sqrt{s} =$ 800 GeV, normalized to the effective weak Born cross section.

infrared-finite remainder containing box diagrams, at LEP/GigaZ it is $\frac{d\sigma_2^{\text{had}}}{d\sigma_0^{\text{weak}}} = 1.65$ per mille, and at $\sqrt{s} = 500$ GeV the corresponding value becomes 4.6 per mille. Everywhere, the pure photonic corrections are the largest one, followed by the $N_f = 1$ corrections. This is, of course, due to the small electron-mass producing large logarithmic mass effects and is extensively discussed in the literature.

VIII. SUMMARY

The NNLO effects of heavy fermions and hadrons on the Bhabha cross sections are accurately known now and the determination of QED two-loop corrections is completed. For each of the corrections there exist several independent calculations. Quite recently, a second determination of the hadronic corrections in [119] fully confirmed our results as presented in [93,114,139] and at our webpage [120]. We indeed checked, when preparing this longer write-up of our results, that, when using the same parametrization [133], all the digits shown in our tables agree with those shown in [119] (see Tables III and IV). The numerical differences which were mentioned in [119] were due to a different choice of the parameter IPAR in [114,119].

Summarizing the numerical discussion, it is quite obvious that for measurements aiming at an accuracy at the per mille level it is crucial to take the heavy-fermion and hadron contributions into account. A detailed conclusion for a specific experiment evidently depends on the experimental setups and will deserve the use of a precise Monte-Carlo program.

Finally, we would like to mention that, in pure QED, not all of the contributions have been determined so far. It would be quite interesting to know also the influence from the so-called radiative loops. This problem was treated in [143], but so far without account of the radiative loop diagram, which include e.g. radiative boxes with the need of knowledge of five-point functions. Also here, final conclusion will be made only with a precise Monte-Carlo program.

As a third field of future improvement we like to mention the complete treatment of electroweak two-loop corrections to Bhabha scattering. As already said there exists some literature on that subject. The leading NNLO weak corrections due to top quarks have been determined long ago in [10]. This was considered as a satisfactory approximation for LEP 1 and implemented e.g. in the packages ZFITTER [81] and in the program family KORALZ [65], KKMC [73,144], BHLUMI [52], BHWIDE [41]; see also the workshop report [145]. An improvement of that might become necessary for large angle scattering at the ILC. This might be done similarly to the recent implementation of weak two-loop corrections for muon pair production in ZFITTER v.6.42 [81], based on original work described in [11,12] and references therein.

ACKNOWLEDGMENTS

We would like to thank B. Kniehl, H. Burkhardt and T. Teubner for help concerning R_{had} and A. Arbuzov, H. Czyz, S.-O. Moch, and K. Mönig for discussions. Work supported by Sonderforschungsbereich/Transregio SFB/TRR 9 of DFG "Computergestützte Theoretische Teilchenphysik," by the Sofja Kovalevskaja Programme of the Alexander von Humboldt Foundation sponsored by the German Federal Ministry of Education and Research, and by the European Community's Marie-Curie Research Training Networks MRTN-CT-2006-035505 HEPTOOLS and MRTN-CT-2006-035482 FLAVIAnet. Feynman diagrams have been drawn with the packages AXODRAW [157] and JAXODRAW [158].

APPENDIX A: ANALYTIC RESULTS FOR THE FERMIONIC VACUUM POLARIZATION

The contribution of a fermion of flavour f to the irreducible renormalized photon vacuum-polarization function

Π, introduced in Eq. (21), can be written in pure QED as

$$\Pi_f(q^2) = \sum_{n=1}^{2}\left(\frac{\alpha}{\pi}\right)^n F_\epsilon^n \left(\frac{m_e^2}{m_f^2}\right)^{n\epsilon} Q_f^{2n} C_f \Pi_f^{(n)}(q^2) + \mathcal{O}(\alpha^3), \tag{A1}$$

where Q_f is the electric-charge quantum number, C_f is the color factor and the normalization factor F_ϵ is defined in Eq. (26).

For our purposes we need both the $n = 1$ and $n = 2$ terms up to $\mathcal{O}(\epsilon^0)$. However, since some components of the infrared-finite differential cross section show single poles in the ϵ plane, we find useful to consider also the $\mathcal{O}(\epsilon)$ part of the one-loop photon self-energy for intermediate checks of the results.

Both expressions can be written in a compact form introducing the variable

$$x = \frac{\sqrt{-q^2 + 4m_f^2} - \sqrt{-q^2}}{\sqrt{-q^2 + 4m_f^2} + \sqrt{-q^2}}. \tag{A2}$$

The results can be found in Appendix A of Ref. [146] and at the webpage [120]. In the spacelike region $-\infty < q^2 < 0$, it is $0 < x < 1$, and one gets a real vacuum polarization:

$$\begin{aligned}\Pi_f^{(1)}(q^2) = &-\frac{5}{9} + \frac{4}{3}\frac{x}{(1-x)^2} + \frac{1}{3}\left[\frac{4}{(1-x)^3} - \frac{6}{(1-x)^2} + 1\right]\ln(x) \\ &+ \frac{\epsilon}{3}\left\{-\frac{28}{9} + \frac{32}{3}\frac{x}{(1-x)^2} + \frac{1}{3}\left[\frac{32}{(1-x)^3} - \frac{48}{(1-x)^2} + \frac{6}{1-x} + 5\right]\ln(x) - 2\left[\frac{4}{(1-x)^3} - \frac{6}{(1-x)^2} + 1\right]\right. \\ &\left.\times\left[\mathrm{Li}_2(-x) + \ln(x)\ln(1+x) - \frac{1}{4}\ln^2(x) + \frac{\zeta_2}{2}\right]\right\},\end{aligned} \tag{A3}$$

$$\begin{aligned}\Pi_f^{(1)}(q^2) = &-\frac{1}{6}\left[\frac{5}{4} - 13\frac{x}{(1-x)^2}\right] + \frac{1}{4}\left[\frac{12}{(1-x)^3} - \frac{18}{(1-x)^2} + \frac{4}{1-x} + 1\right]\ln(x) - \frac{4}{3}\left[\frac{4}{(1-x)^3} - \frac{6}{(1-x)^2} + 1\right] \\ &\times\left\{\mathrm{Li}_2(-x) + \frac{1}{2}\mathrm{Li}_2(x) + \ln(x)\left[\ln(1+x) + \frac{1}{2}\ln(1-x)\right]\right\} \\ &- \frac{1}{6}\left[\frac{7}{(1-x)^4} - \frac{26}{(1-x)^3} + \frac{23}{(1-x)^2} + \frac{2}{1-x} - 6\right]\ln^2(x) + \frac{1}{3}\left[\frac{4}{(1-x)^4} - \frac{8}{(1-x)^3} + \frac{4}{(1-x)^2} - 1\right] \\ &\times\{\ln^2(x)[\ln(1-x) + 2\ln(1+x)] + 4\ln(x)[\mathrm{Li}_2(x) + 2\mathrm{Li}_2(-x)] - 6[\mathrm{Li}_3(x) + 2\mathrm{Li}_3(-x)] - 3\zeta_3\}.\end{aligned} \tag{A4}$$

For the timelike region, we have to perform an analytical continuation to $q^2 > 4m_f^2$ by setting $q^2 \to q^2 + i\delta$ in Eq. (A2). Now, the conformal variable x develops a small positive imaginary part and it is $-1 < \mathrm{Re}x < 0$. In order to derive $\mathrm{Im}\Pi$ of Eq. (23), we may introduce an auxiliary variable y:

$$y = \frac{\sqrt{q^2} - \sqrt{-q^2 - 4m_f^2}}{\sqrt{q^2} + \sqrt{q^2 - 4m_f^2}} \tag{A5}$$

and observe that $x = -y + i\delta$, with $y = 0$ for $q^2 \to \infty$ and $y = 1$ for $q^2 = 4m_f^2$. With these conventions, it becomes evident for Eqs. (A3) and (A4) that $\mathrm{Li}_2(\pm x)$, $\mathrm{Li}_3(\pm x)$, and $\ln(1+x)$, and $\ln(1+x)$ stay well defined, and one has to take care about $\ln(x)$:

$$\ln(x) \to \ln(-y + i\delta) = \ln(y) + i\pi. \tag{A6}$$

Of course, one may perform the evaluations with complex variables either.

The contribution of electron loops to the irreducible renormalized photon vacuum-polarization function Π of Eq. (21) in the small electron-mass limit is available in pure QED up to three loops,

$$\Pi_e(q^2) = \sum_{n=1}^{3}\left(\frac{\alpha}{\pi}\right)^n \Pi_e^{(n)}(q^2) + \mathcal{O}(\alpha^4). \tag{A7}$$

The one- and two-loop contributions can be obtained by expanding Eqs. (A3) and (A4) and neglecting terms suppressed by positive powers of the electron mass. The three-loop component, (we do not include double-bubble diagrams with two different flavors), can be found in Eqs. (7) and (9) of Ref. [126]. The results for $q^2 < 0$ are:

$$\Pi_e^{(1)}(q^2) = -\frac{5}{9} - \frac{1}{3}\ln\left(-\frac{m_e^2}{q^2}\right) + \mathcal{O}(m_e^2), \tag{A8}$$

$$\Pi_e^{(2)}(q^2) = -\frac{5}{24} + \zeta_3 - \frac{1}{4}\ln\left(-\frac{m^2}{q^2}\right) + \mathcal{O}(m_e^2), \tag{A9}$$

$$\Pi_e^{(3)}(q^2) = \frac{121}{192} - \left[2\ln(2) - \frac{5}{4}\right]\zeta_2 + \frac{99}{64}\zeta_3 - \frac{5}{2}\zeta_5 + \frac{1}{32}\ln\left(-\frac{m_e^2}{q^2}\right) + \underbrace{\frac{307}{864} + \frac{2}{3}\zeta_2 - \frac{545}{576}\zeta_3 + \left(\frac{11}{24} - \frac{\zeta_3}{3}\right)\ln\left(-\frac{m_e^2}{q^2}\right) + \frac{1}{24}\ln^2\left(-\frac{m_e^2}{q^2}\right)}_{\text{double electron bubble}} + \mathcal{O}(m_e^2). \tag{A10}$$

The continuation to $q^2 > 0$ is again obtained by the replacement $q^2 \to q^2 + i\delta$.

APPENDIX B: MASTER INTEGRALS FOR THE BOX KERNEL FUNCTIONS

The three kernel functions for irreducible box diagrams of Fig. 7 may be found at webpage [120] with their exact dependences on m_e and on ϵ. They are expressed by eight master integrals, which were evaluated in the limit $m_e^2 \ll z, s, |t|, |u|$. The master integrals of Eq. (70), for $x = s$ and $y = t$, are evaluated to the power in ϵ needed here:

$$M^{(1)} = N\int \frac{d^Dk}{(k^2 - m_e^2)} = m_e^2\left[\frac{1}{\epsilon} + 1 + \epsilon\left(1 + \frac{\zeta_2}{2}\right)\right], \tag{B1}$$

$$M^{(2)} = N\int \frac{d^Dk}{(k^2 - m_e^2)[(k - p_1 - p_2)^2 - m_e^2]} = \frac{1}{\epsilon} + 2 + \ln\left(-\frac{m_e^2}{s}\right) + \epsilon\left[4 - \frac{\zeta_2}{2} + 2\ln\left(-\frac{m_e^2}{s}\right) + \frac{1}{2}\ln^2\left(-\frac{m_e^2}{s}\right)\right] + \mathcal{O}(m_e^2), \tag{B2}$$

$$M^{(3)} = N\int \frac{d^Dk}{k^2(k - p_1 + p_3)^2} = \frac{1}{\epsilon} + 2 + \ln\left(-\frac{m_e^2}{t}\right), \tag{B3}$$

$$M^{(4)} = N\int \frac{d^Dk}{(k^2 - m_e^2)[(k - p_3)^2 - z]}, = \mathcal{O}(m_e^0), \tag{B4}$$

$$M^{(5)} = N\int \frac{d^Dk}{(k^2 - z)(k - p_1 + p_3)^2} = \frac{1}{\epsilon} + 2 + \ln\left(-\frac{m_e^2}{t}\right) - \ln\left(1 - \frac{z}{t}\right) - \frac{z}{t}\left[\ln\left(-\frac{z}{t}\right) - \ln\left(1 - \frac{z}{t}\right)\right], \tag{B5, B6}$$

$$M^{(6)} = N\int \frac{d^Dk}{(k^2 - z)[(k + p_3)^2 - m_e^2][(k + p_3 - p_1 - p_2)^2 - m_e^2]} = \frac{1}{s}\left[\zeta_2 + \frac{1}{2}\ln^2\left(-\frac{z}{s}\right) + \mathrm{Li}_2\left(1 + \frac{z}{s}\right)\right] + \mathcal{O}(m_e^2), \tag{B7}$$

$$M^{(7)} = N\int \frac{d^Dk}{(k^2 - z)[(k + p_3)^2 - m_e^2](k + p_3 - p_1)^2} = \frac{1}{t}\left\{\zeta_2 + \ln\left(-\frac{z}{t}\right)\left[\ln\left(-\frac{m_e^2}{t}\right) - \frac{1}{2}\ln\left(-\frac{z}{t}\right)\right] - \ln\left(1 - \frac{z}{t}\right)\left[\ln\left(-\frac{m_e^2}{t}\right) - \ln\left(-\frac{z}{t}\right)\right] + \mathrm{Li}_2\left(\frac{z}{t}\right)\right\} + \mathcal{O}(m_e^2), \tag{B8}$$

$$M^{(8)} = N\int \frac{d^Dk}{(k^2 - z)[(k + p_3)^2 - m_e^2](k + p_3 - p_1)^2[(k + p_3 - p_1 - p_2)^2 - m_e^2]} = \frac{1}{s(t - z)}\left\{\frac{1}{\epsilon}\left[\ln\left(-\frac{m_e^2}{t}\right) + \ln\left(-\frac{z}{s}\right) - \ln\left(-\frac{z}{t}\right)\right] - 2\zeta_2 + \ln\left(-\frac{m_e^2}{t}\right)\left[\frac{1}{2}\ln\left(-\frac{m_e^2}{t}\right) + \ln\left(-\frac{z}{s}\right) + \ln\left(-\frac{z}{t}\right) - 2\ln\left(1 - \frac{z}{t}\right)\right] - \frac{3}{2}\ln^2\left(-\frac{z}{t}\right) + \ln\left(-\frac{z}{s}\right)\ln\left(-\frac{z}{t}\right) - 2\ln\left(1 - \frac{z}{t}\right)\left[\ln\left(-\frac{z}{s}\right) - \ln\left(-\frac{z}{t}\right)\right] - \mathrm{Li}_2\left(1 + \frac{z}{s}\right)\right\} + \mathcal{O}(m_e^2). \tag{B9}$$

where $D = 4 - 2\epsilon$ and

$$N = m_e^{2\epsilon} \frac{e^{\gamma_E \epsilon}}{i\pi^{2-\epsilon}}. \tag{B10}$$

For $M^{(1)}$ and $M^{(2)}$, results are needed up to $\mathcal{O}(\epsilon)$, since, after the reduction procedure, both coefficients $c_i^{(1)}$ and $c_i^{(2)}$, for $i = A, B, C$, include terms $\mathcal{O}(\epsilon^{-1})$. For all other basis integrals, $\mathcal{O}(\epsilon^0)$ results suffice. Note that for $M^{(1)}$ (tadpole), $M^{(3)}$ and $M^{(5)}$ (no dependence on m_e, apart from the normalization factor N) results are exact. In other cases, the order of the expansion in me depends on the coefficients $c_i^{(j)}$. For example, we have $c_i^{(2)} = \mathcal{O}(m_e^{-2})$, and we compute $M^{(2)}$ up to $\mathcal{O}(m_e^0)$ (note the overall factor m_e^2 in Eq. (65)). In contrast, we have $c_i^{(4)} = \mathcal{O}(m_e^0)$ and we do not need $M^{(4)}$ up to $\mathcal{O}(m_e^0)$.

APPENDIX C: SOFT REAL PHOTON EMISSION

The leading order contributions to the soft real photon corrections

$$e^-(p_1) + e^+(p_2) \to e^-(p_3) + e^+(p_4) + \gamma(k) \tag{C1}$$

to the Bhabha cross section (2) are contained in the factor F_{soft}:

$$\frac{d\sigma^{\text{LO}}}{d\Omega} = \frac{d\sigma_0}{d\Omega} \frac{\alpha}{\pi} F_{\text{soft}}(\omega_{,s,t,m_e^2)}, \tag{C2}$$

with ω being the upper limit of the energy of the non-observed soft photons:

$$E_\gamma \in [0, \omega]. \tag{C3}$$

The ω has to be chosen as small as to guaranty that the emitted photon does not change the kinematics of the process (1). The NLO radiative cross section with $\mathcal{O}(\alpha)$ vacuum polarization insertions is:

$$\begin{aligned}\frac{d\sigma_\gamma^{\text{NLO}}}{d\Omega} = \frac{\alpha^2}{s}\Bigg\{ & \frac{v_1(s,t)}{s^2} \text{Re}\Pi^{(1)}(s) \\ & + \frac{v_2(s,t)}{st} \text{Re}[\Pi^{(1)}(s) + \Pi^{(1)}(t)] \\ & + \frac{v_1(t,s)}{t^2} \text{Re}\Pi^{(1)}(t)\Bigg\}\left(\frac{\alpha}{\pi}\right) F_{\text{soft}}(\omega, s, t, m_e^2).\end{aligned} \tag{C4}$$

The result for the soft photon factor is split into initial and final state radiation and their interference:

$$F_{\text{soft}}(\omega, s, t, m_e^2) = \delta_{\text{ini}} + \delta_{\text{int}} + \delta_{\text{fin}}, \tag{C5}$$

where

$$\delta_{\text{ini}} = (Q_1^2 + Q_2^2)F_{11} + Q_1 Q_2 F_{12} = 2F_{11} + F_{12}, \tag{C6}$$

$$\begin{aligned}\delta_{\text{int}} &= (Q_1 Q_3 + Q_2 Q_4)F_{13} + (Q_1 Q_4 + Q_2 Q_3)F_{14} \\ &= 2F_{13} + 2F_{14}.\end{aligned} \tag{C7}$$

$$\delta_{\text{fin}} = (Q_3^2 + Q_4^2)F_{33} + Q_3 Q_4 F_{34} = 2F_{33} + F_{34}. \tag{C8}$$

Each of the terms in Eqs. (C6)–(C8) exhibits the radiating particles—a factor $Q_i Q_j$ marks the emission of the photons from particles with momenta p_i and p_j; Of course, it is $Q_i Q_j = 1$ here. Since the initial and final state particles have equal masses, it is additionally:

$$F_{33} = F_{11}. \tag{C9}$$

$$F_{34} = F_{12}. \tag{C10}$$

So, it will be:

$$F_{\text{soft}}(\omega, s, t, m_e^2) = 4F_{11} + 2F_{12} + 2F_{13} + 2F_{14}. \tag{C11}$$

The evaluation of F_{soft} follows standard textbook methods (see e.g. for details in Sec. (4.3) of [147]). The exact result for the soft radiation functions is, for $d = 4 - 2\epsilon$:

$$F_{11} = \Delta_\epsilon + \frac{1}{2\beta} \log\left(\frac{1+\beta}{1-\beta}\right), \tag{C12}$$

$$\begin{aligned}F_{12} = {} & \Delta_\epsilon\left[-\frac{2(s-2m^2)}{s\beta} \log\left(\frac{1+\beta}{1-\beta}\right)\right] \\ & + \frac{2(s-2m^2)}{s\beta}\left[\text{Li}_2\left(\frac{2\beta}{\beta-1}\right) - \text{Li}_2\left(\frac{2\beta}{\beta+1}\right)\right],\end{aligned} \tag{C13}$$

$$F_{13} = \Delta_\epsilon\left(-\frac{T}{\sqrt{\lambda_T}}\right) \ln\left(\frac{T+\sqrt{\lambda_T}}{T-\sqrt{\lambda_T}}\right) + F_{13}^{\text{fin}}, \tag{C14}$$

$$F_{14} = -F_{13} \quad \text{with } (t \leftrightarrow u), \tag{C15}$$

and

$$\begin{aligned}F_{13}^{\text{fin}} = \frac{(t-2m^2)}{t\beta_t}\Bigg[& \text{Li}_2\left(\frac{\beta - 1/\beta_t}{1+\beta}\right) - \text{Li}_2\left(\frac{\beta + 1/\beta_t}{1+\beta}\right) \\ & - \text{Li}_2\left(-\frac{\beta - 1/\beta_t}{1-\beta}\right) + \text{Li}_2\left(\frac{\beta+1}{1-\beta}\right) \\ & + \text{Li}_2\left(-\frac{\beta + 1/\beta_t}{1-\beta}\right)\Bigg].\end{aligned} \tag{C16}$$

We use the abbreviations:

$$\beta = \sqrt{1 - 4m^2/s}, \tag{C17}$$

$$\beta_t = \sqrt{1 - 4m^2/t}, \tag{C18}$$

$$T = 2m^2 - t, \tag{C19}$$

$$\sqrt{\lambda_T} = \sqrt{T^2 - 4m^4}, \tag{C20}$$

$$\beta_u = \sqrt{1 - 4m^2/u}, \tag{C21}$$

$$U = 2m^2 - u, \tag{C22}$$

$$\sqrt{\lambda_U} = \sqrt{U^2 - 4m^4}. \tag{C23}$$

Our kinematics fulfills here $s + t + u = 4m^2$, and it is T, $U > 0$. If necessary, the logarithms and dilogarithms may be analytically continued with the replacement

$$s \to s + i\epsilon, \tag{C24}$$

e.g.

$$\mathrm{Li}_2\left(\frac{2\beta}{\beta - 1}\right) = -\mathrm{Li}_2\left(\frac{\beta - 1}{2\beta}\right) - \mathrm{Li}_2(1) - \frac{1}{2}\ln^2\left(\frac{2\beta}{1 - \beta}\right). \tag{C25}$$

In the limit of small electron mass m_e, this simplifies considerably ($\hat{s} = s/m_e^2$):

$$F_{11} = \Delta_\epsilon + \tfrac{1}{2}\ln(\hat{s}), \tag{C26}$$

$$F_{12} = -2\Delta_\epsilon \ln(\hat{s}) - \tfrac{1}{2}\ln(\hat{s})^2 - 2\zeta_2, \tag{C27}$$

$$F_{13} = -2\Delta_\epsilon \ln\left(-\frac{t}{m_e^2}\right) - \frac{1}{2}\ln(\hat{s})^2 - 2\zeta_2 - \mathrm{Li}_2\left(-\frac{u}{t}\right), \tag{C28}$$

$$F_{14} = 2\Delta_\epsilon \ln\left(-\frac{u}{m_e^2}\right) + \frac{1}{2}\ln(\hat{s})^2 + 2\zeta_2 + \mathrm{Li}_2\left(-\frac{t}{u}\right). \tag{C29}$$

Finally, the divergent part is:

$$\Delta_\epsilon = \frac{1}{2}\left[\frac{F_\epsilon}{\epsilon} - \ln(\hat{s})\right] - \ln\left(\frac{2\omega}{\sqrt{s}}\right). \tag{C30}$$

Taking all the terms together, we obtain:

$$\begin{aligned} F_{\mathrm{soft}}(\omega, s, t, m_e^2) = &\left[\frac{F_\epsilon}{\epsilon} - \ln(\hat{s}) - 2\ln\left(\frac{2\omega}{\sqrt{s}}\right)\right] \\ &\times \left[-2\ln(\hat{s}) + 2 - 2\ln\left(\frac{t}{u}\right)\right] - \ln(\hat{s})^2 \\ &- 4\zeta_2 + 2\ln(\hat{s}) + 2\mathrm{Li}_2\left(-\frac{u}{t}\right). \end{aligned} \tag{C31}$$

This expression agrees, of course, with e.g. Eq. (4.5) of [113].

APPENDIX D: REAL FERMION PAIR OR HADRON EMISSION

The numerical influence of the virtual corrections gets modified by the nonobserved emission of real pairs of electrons or other fermions, or of hadrons:

$$\frac{d\sigma^{\mathrm{real}}}{d\Omega} = \frac{d\sigma_0}{d\Omega}\frac{\alpha^2}{\pi^2}[\delta^e + \delta^f + \delta^{\mathrm{had}}]. \tag{D1}$$

The real pairs or hadrons give nonsingular contributions and depend, in the simplest configuration, on an energetic cutoff D on the invariant mass of the nonobserved pair or hadrons E_{real}, and of course also on the production threshold $2M$.

There are two basically different situations. In case $4M^2 \ll s$, $|t|$, $|u|$, one may additionally choose $2M < E_{\mathrm{real}} < DE_{\mathrm{beam}} \ll E_{\mathrm{beam}}$ (remember $E_{\mathrm{beam}} = \sqrt{s}/2$), and observes a logarithmic dependence of the cross sections on the two parameters M, D. In the other case, assuming $M \gg m_e$ but otherwise arbitrary, as it is done in the present study if not stated differently, the concept of soft pairs becomes senseless and one has to evaluate the pair and hadron emission cross section numerically with MC methods.

For completeness and because of the numerical importance, we will include the soft pair emission contributions for electrons, which is by far the biggest one. For this case, analytical expressions with logarithmic accuracy are known from [44]:

$$\begin{aligned} \delta^e_{\mathrm{soft}} = &\tfrac{1}{3}[\tfrac{1}{3}L_s^3 + L_s^2(2\ln(D) - \tfrac{5}{3}) + L_s(4\ln^2(D) - \tfrac{20}{3}\ln(D) \\ &+ A_s) + \tfrac{1}{3}L_t^3 + L_t^2(2\ln(D) - \tfrac{5}{3}) + L_t(4\ln^2(D) \\ &- \tfrac{20}{3}\ln(D) + A_t) - \tfrac{1}{3}L_u^3 - L_u^2(2\ln(D) - \tfrac{5}{3}) \\ &- L_u(4\ln^2(D) - \tfrac{20}{3}\ln(D) + A_u)], \end{aligned} \tag{D2}$$

where

$$L_s = \ln\left(\frac{s}{m_s^2}\right), \tag{D3}$$

$$L_\upsilon = \ln\left(-\frac{\upsilon}{m_e^2}\right), \qquad \upsilon = t, u, \tag{D4}$$

$$A_s = \tfrac{56}{9} - 4\zeta_2. \tag{D5}$$

$$A_\upsilon = A_s + 2\mathrm{Li}_2\left(\frac{1 \pm \cos\theta}{2}\right), \qquad \upsilon = t, u. \tag{D6}$$

The parameter D has to fulfill:

$$2m_e \ll DE_{\mathrm{beam}} \ll E_{\mathrm{beam}}. \tag{D7}$$

From the sum of (39) and (D1), the compensation of the leading mass singularities (contained here in the L_s^3, L_t^3, L_u^3 terms) in the cross section becomes evident.

APPENDIX E: THE CROSS-SECTION RATIO R_{had}

The numerical values of the irreducible two-loop corrections depend crucially on $R_{\mathrm{had}}(s)$ as defined in (28), while the reducible corrections may be evaluated with one of the publicly available parametrizations of $\Pi(q^2)$ [see (22)]. Unfortunately, we did not find an actual, publicly available code for $R_{\mathrm{had}}(s)$ that covers the complete integration region from the threshold at $s = 4M_\pi^2$ to infinity. In our short communication [93], we used the Fortran routine of H. Burkhardt [133]. This parameterization dates back to 1986 and was used for the numerics in [124], and it was available by contacting the author [133]. The Fortran

file is made available at our website [120]. It is to be expected that current hadronic data would not induce changes compared to the parametrization of [133] of more than about 10%. This would be tolerable in view of the smallness of the irreducible two-loop contributions in our analysis. For the numerically much more sensitive reducible contributions, the running coupling $\alpha_{\rm em}$ is needed, and implementations of that are publicly available, e.g. the Fortran package HADR5.F at [132].

For the present study, we improved our numerical basis for the evaluation of the irreducible vertex and box contributions by combining packages for the evaluation of $R_{\rm had}(s)$ in different kinematical regions:

(A) From threshold at $s = 4m_\pi^2$ to $s = 0.03$ GeV^2: We follow Sec. 8.1 of [148]:

$$R_{\rm had}(s) = R_{\pi^+\pi^-}(s) = \frac{1}{4}\left(1 - \frac{4m_\pi^2}{s}\right)^{3/2} |F_\pi(s)|^2, \tag{E1}$$

$$F_\pi(s) = 1 + 1.879\left(\frac{s}{\rm GeV^2}\right) + 3.3\left(\frac{s}{\rm GeV^2}\right)^2 - 0.7\left(\frac{s}{\rm GeV^2}\right)^3. \tag{E2}$$

The above is based on a fit to e^+e^- data whose results are shown in Table 3 of [148]; spacelike data [149] are also taken into account.

(B) From $s = 0.03$ GeV^2 to $s = 10\,000$ GeV^2: Use of subroutine [150].

(C) Above $s = 10\,000$ GeV^2: Use of subroutine RHAD.FV.1.00, published in [152].

In Fig. 15 we show the $R_{\rm had}$ resulting from our Fortran implementation for the regions (A) to (C) as described above.

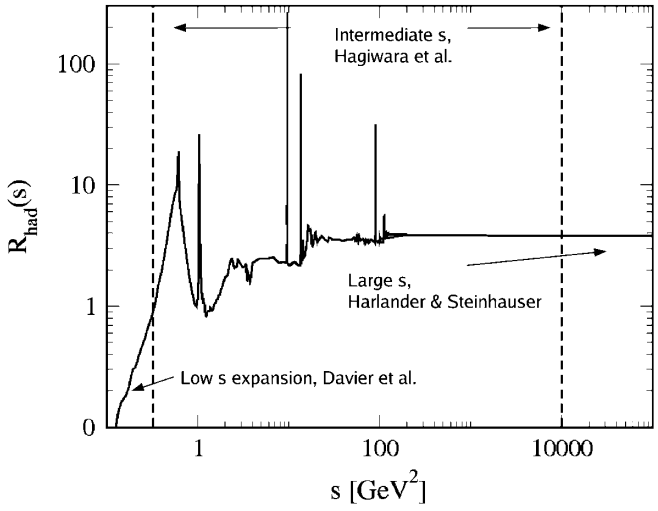

FIG. 15. The implementation of $R_{\rm had}$ used for the numerical evaluation of irreducible two-loop corrections.

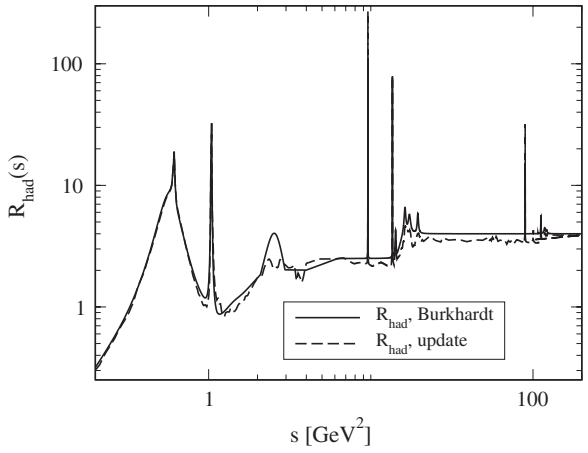

FIG. 16. A comparison of the parametrizations from [133,150].

In Fig. 16 we compare the implementation of $R_{\rm had}(s)$ taken from Burkhardt [133] ($R_{\rm had,I}$) and our parametrization based on [148,150,152] ($R_{\rm had,II}$). As already stated, the deviations are evidently much smaller than one might expect and may be considered to be irrelevant here.

We close this section with a brief discussion of narrow resonances. Narrow resonances are implemented replacing the rapidly varying cross-section ratio with the parametrization

$$R_{\rm res}(z) = \frac{9\pi}{\alpha^2} M_{\rm res}\Gamma^{e^+e^-}\delta(z - M_{\rm res}^2). \tag{E3}$$

The integration over z is then carried on analytically leading to the following result for the IR-finite remainder (including the irreducible box diagrams) of Eq. (87):

TABLE V. Numerical values for the treatment of narrow resonances, taken directly from [133].

resonance	$M_{\rm res}$ [GeV]	$\Gamma_{\rm res}^{e^+e^-}$ [keV]
$\omega(782)$	0.7826	0.66
$\phi(1020)$	1.0195	1.31
$J/\psi(1S)$	3.0969	4.7
$\psi(2S)$	3.6860	2.1
$\psi(3770)$	3.7699	0.26
$\psi(4040)$	4.0300	0.75
$\psi(4160)$	4.1590	0.77
$\psi(4415)$	4.4150	0.47
$\Upsilon(1S)$	9.4600	1.22
$\Upsilon(2S)$	10.0234	0.54
$\Upsilon(3S)$	10.3555	0.40
$\Upsilon(4S)$	10.577	0.24
$\Upsilon(10860)$	10.865	0.31
$\Upsilon(11020)$	11.019	0.13

$$\frac{d\bar{\sigma}_{\rm rest}}{d\Omega} = \frac{9\pi}{\alpha^2}\frac{\Gamma_{\rm res}^{e^+e^-}}{M_{\rm res}}\left\{\frac{F_1(M_{\rm res}^2)}{t-M_{\rm res}^2}+\frac{1}{s-M_{\rm res}^2}\right.$$
$$\left.\times\left[F_2(M_{\rm res}^2)+F_3(M_{\rm res}^2)\ln\left|1-\frac{M_{\rm res}^2}{s}\right|\right]\right\}. \quad \text{(E4)}$$

For the numerical evaluation of the contribution due to the narrow resonances, we use the values listed in the Burkhardt's routine [133], collected in Table V.

APPENDIX F: EVALUATION OF POLYLOGARITHMS

At several instances, dilogarithms $\mathrm{Li}_2(z)$ and trilogarithms $\mathrm{Li}_3(z)$ of complex argument are needed. A definition of polylogarithms is:

$$\mathrm{Li}_n(z) = S_{n-1,1}(z) = \frac{(-1)^n}{(n-2)!}\int_0^1 \frac{dt}{t}\ln^{n-2}(t)\ln(1-zt). \quad \text{(F1)}$$

They have the special values $\mathrm{Li}_n(0)=0$ and $\mathrm{Li}_n(1)=\zeta(n)$, where $\zeta(s)$ is the Riemann ζ-function, $\zeta(2)=\pi^2/6$, $\zeta(3)=1.202\,056\,903\,159\,594\,285\,4\ldots$. An efficient evaluation transforms the arguments to the region where modulus and real part are bound: $|z|\le 1$ and $\Re e(z)<\frac{1}{2}$, using:

$$\mathrm{Li}_2(z) = -\mathrm{Li}_2\left(\frac{1}{z}\right)-\frac{1}{2}\ln^2(-z)-\zeta(2), \quad \text{(F2)}$$

$$\mathrm{Li}_2(z) = -\mathrm{Li}_2(1-z)+\zeta(2)-\ln(z)\ln(1-z), \quad \text{(F3)}$$

and

$$\mathrm{Li}_3(z) = \mathrm{Li}_3\left(\frac{1}{z}\right)-\frac{1}{6}\ln^3(-z)-\zeta(2)\ln(-z), \quad \text{(F4)}$$

$$\mathrm{Li}_3(z) = -\mathrm{Li}_3\left(1-\frac{1}{z}\right)-\mathrm{Li}_3(1-z)+\zeta(3)+\frac{1}{6}\ln^3(z)$$
$$+\zeta(2)\ln(z)-\frac{1}{2}\ln^2(z)\ln(1-z). \quad \text{(F5)}$$

Then, series expansions with Bernoulli numbers ensure rapid convergence. For $\mathrm{Li}_2(z)$ we follow Appendix A of [153]:

$$\mathrm{Li}_2(z) = \sum_{j=0}^{\infty}\frac{B_j}{(j+1)!}[-\ln(1-z)]^{j+1}$$
$$= -\ln(1-z)-\frac{1}{4}\ln^2(1-z)$$
$$+4\pi\sum_{j=1}^{\infty}\zeta(2j)\frac{(-1)^j}{2j+1}\left[\frac{\ln(1-z)}{2\pi}\right]^{2j+1}. \quad \text{(F6)}$$

The B_j are Bernoulli numbers, $B_0=1$, etc. Useful series expansions for $\mathrm{Li}_n(z)$ are given in Eqs. (48) and (49) of [154], which we reproduce here for the special case $n=3$:

$$\mathrm{Li}_3(z) = \sum_{j=0}^{\infty}\frac{C_3(j)}{(j+1)!}[-\ln(1-z)]^{j+1}, \quad \text{(F7)}$$

$$C_3(j) = \sum_{k=0}^{j}\binom{j}{k}\frac{B_{j-k}B_k}{1+k}, \quad \text{(F8)}$$

with $C_3(0)=1$ etc. For $\mathrm{Li}_2(z)$ and $\mathrm{Li}_3(z)$ we observe typically that n summation terms give an $n\pm 1$ digits accuracy. We just mention that we do not allow to evaluate the logarithms and polylogarithms at their cuts (negative real axis beginning at $z=0$ and positive real axis beginning at $z=1$, respectively). For other conventions we refer to the corresponding remark at p. 19 of [154]. Our Fortran code is available as file cpolylog.f at the website [120].

An alternative, efficient algorithm for the evaluation of polylogarithms is described in [155,156].

[1] H. Bhabha, Proc. R. Soc. A **154**, 195 (1936).
[2] M. Consoli, Nucl. Phys. **B160**, 208 (1979).
[3] M. Consoli, M. Greco, and S. Lo Presti, Phys. Lett. **113B**, 415 (1982).
[4] M. Caffo, R. Gatto, and E. Remiddi, Nucl. Phys. **B252**, 378 (1985).
[5] M. Böhm *et al.*, Phys. Lett. **144B**, 414 (1984).
[6] K. Tobimatsu and Y. Shimizu, Prog. Theor. Phys. **75**, 905 (1986).
[7] K. Tobimatsu and Y. Shimizu, Prog. Theor. Phys. **74**, 567 (1985).
[8] M. Böhm, A. Denner, and W. Hollik, Nucl. Phys. **B304**, 687 (1988).
[9] F. Berends, R. Kleiss, and W. Hollik, Nucl. Phys. **B304**, 712 (1988).
[10] D. Bardin, W. Hollik, and T. Riemann, Z. Phys. C **49**, 485 (1991).
[11] M. Awramik, M. Czakon, A. Freitas, and G. Weiglein, Phys. Rev. D **69**, 053006 (2004).
[12] M. Awramik, M. Czakon, and A. Freitas, J. High Energy Phys. 11 (2006) 048.
[13] F. Berends and G. Komen, Phys. Lett. **63B**, 432 (1976).

[14] F. Berends and R. Kleiss, Nucl. Phys. **B228**, 537 (1983).
[15] F. A. Berends, P. H. Daverveldt, and R. Kleiss, Nucl. Phys. **B253**, 421 (1985).
[16] M. Greco, Phys. Lett. B **177**, 97 (1986).
[17] S. Kuroda *et al.*, Comput. Phys. Commun. **48**, 335 (1988).
[18] D. Karlen, Nucl. Phys. **B289**, 23 (1987).
[19] F. Aversa *et al.*, Phys. Lett. B **247**, 93 (1990).
[20] J. Fujimoto *et al.*, Prog. Theor. Phys. Suppl. **100**, 1 (1990).
[21] M. Caffo, H. Czyz, and E. Remiddi, Nuovo Cimento Soc. Ital. Fis. A **105**, 277 (1992).
[22] M. Cacciari *et al.*, Phys. Lett. B **268**, 441 (1991).
[23] M. Cacciari *et al.*, Phys. Lett. B **271**, 431 (1991).
[24] W. Beenakker, F. A. Berends, and S. C. van der Marck, Nucl. Phys. **B349**, 323 (1991).
[25] W. Beenakker, F. A. Berends, and S. C. van der Marck, Nucl. Phys. **B355**, 281 (1991).
[26] F. Aversa and M. Greco, Phys. Lett. B **271**, 435 (1991).
[27] S. Riemann, Report No. PHE-91-04, 1991.
[28] V. S. Fadin *et al.*, JINR Report No. JINR-E2-92-577, 1992.
[29] K. S. Bjoerkevoll, P. Osland, and G. Faeldt, Nucl. Phys. **B386**, 280 (1992).
[30] K. S. Bjoerkevoll, P. Osland, and G. Faeldt, Nucl. Phys. **B386**, 303 (1992).
[31] D. Y. Bardin *et al.*, arXiv:hep-ph/9412201.
[32] G. Montagna *et al.*, Nucl. Phys. **B401**, 3 (1993).
[33] M. Caffo, E. Remiddi, and H. Czyz, Int. J. Mod. Phys. C **4**, 591 (1993).
[34] J. Fujimoto, Y. Shimizu, and T. Munehisa, Prog. Theor. Phys. **91**, 333 (1994).
[35] M. Caffo, H. Czyz, and E. Remiddi, Phys. Lett. B **327**, 369 (1994).
[36] M. Caffo, E. Remiddi, and H. Czyz, CERN Report No. 95-03 (1994), pp. 361–368.
[37] V. S. Fadin *et al.*, Proc. of the 29th International Conference on Small angle Bhabha scattering with a 0.1% accuracy, Rencontres de Moriond, 1994, p. 161.
[38] A. Arbuzov *et al.*, arXiv:hep-ph/9506323.
[39] M. Cacciari *et al.*, Comput. Phys. Commun. **90**, 301 (1995).
[40] J. H. Field and T. Riemann, Comput. Phys. Commun. **94**, 53 (1996).
[41] S. Jadach, W. Placzek, and B. F. L. Ward, Phys. Lett. B **390**, 298 (1997).
[42] A. Arbuzov *et al.*, Nucl. Phys. **B485**, 457 (1997).
[43] A. B. Arbuzov *et al.*, Nucl. Phys. **B474**, 271 (1996).
[44] A. B. Arbuzov *et al.*, Phys. At. Nucl. **60**, 591 (1997).
[45] M. Caffo, H. Czyz, and E. Remiddi, Phys. Lett. B **378**, 357 (1996).
[46] M. Caffo and H. Czyz, Comput. Phys. Commun. **100**, 99 (1997).
[47] A. Arbuzov *et al.*, Nucl. Phys. B, Proc. Suppl. **51**, 154 (1996).
[48] A. Arbuzov *et al.*, Phys. Lett. B **394**, 218 (1997).
[49] A. B. Arbuzov *et al.*, Nucl. Phys. **B483**, 83 (1997).
[50] A. B. Arbuzov *et al.*, Phys. Lett. B **399**, 312 (1997).
[51] S. Jadach *et al.*, Nucl. Phys. B, Proc. Suppl. **51C**, 164 (1996).
[52] S. Jadach *et al.*, Comput. Phys. Commun. **102**, 229 (1997).
[53] S. Jadach *et al.*, arXiv:hep-ph/9602393.
[54] S. Jadach *et al.*, Phys. Lett. B **377**, 168 (1996).
[55] W. Beenakker and G. Passarino, Phys. Lett. B **425**, 199 (1998).
[56] M. Caffo, H. Czyz, and E. Remiddi, Nuovo Cimento Soc. Ital. Fis. A **110**, 515 (1997).
[57] A. Arbuzov *et al.*, J. High Energy Phys. 10 (1997) 001.
[58] N. P. Merenkov *et al.*, Acta Phys. Pol. B **28**, 491 (1997).
[59] A. Arbuzov, E. Kuraev, and B. Shaikhatdenov, Mod. Phys. Lett. A **13**, 2305 (1998).
[60] G. Montagna *et al.*, Nucl. Phys. **B547**, 39 (1999).
[61] A. B. Arbuzov, E. A. Kuraev, and B. G. Shaikhatdenov, J. Exp. Theor. Phys. **88**, 213 (1999); **97**, 858(E) (2003).
[62] D. Bardin *et al.*, Comput. Phys. Commun. **133**, 229 (2001).
[63] A. Arbuzov, arXiv:hep-ph/9907298.
[64] W. Placzek *et al.*, arXiv:hep-ph/9903381.
[65] S. Jadach, B. F. L. Ward, and Z. Was, Comput. Phys. Commun. **124**, 233 (2000).
[66] G. Montagna, O. Nicrosini, and F. Piccinini, Phys. Lett. B **460**, 425 (1999).
[67] C. M. Carloni Calame *et al.*, arXiv:hep-ph/0001131.
[68] V. Antonelli, E. A. Kuraev, and B. G. Shaikhatdenov, Nucl. Phys. **B568**, 40 (2000).
[69] C. C. Calame *et al.*, Nucl. Phys. **B584**, 459 (2000).
[70] M. Battaglia, S. Jadach, and D. Bardin, eConf C010630 E3015 (2001).
[71] C. M. Carloni Calame, Phys. Lett. B **520**, 16 (2001).
[72] D. Karlen and H. Burkhardt, Eur. Phys. J. C **22**, 39 (2001).
[73] B. F. L. Ward, S. Jadach, and Z. Was, Nucl. Phys. B, Proc. Suppl. **116**, 73 (2003).
[74] S. Jadach, arXiv:hep-ph/0306083.
[75] A. Arbuzov *et al.*, Eur. Phys. J. C **34**, 267 (2004).
[76] M. Czakon, J. Gluza, and T. Riemann, arXiv:hep-ph/0409017.
[77] J. Fleischer, A. Lorca, and T. Riemann, arXiv:hep-ph/0409034.
[78] J. Gluza, A. Lorca, and T. Riemann, Nucl. Instrum. Methods Phys. Res., Sect. A **534**, 289 (2004).
[79] A. Lorca and T. Riemann, Nucl. Phys. B, Proc. Suppl. **135**, 328 (2004).
[80] A. B. Arbuzov *et al.*, Eur. Phys. J. C **46**, 689 (2006).
[81] A. Arbuzov *et al.*, Comput. Phys. Commun. **174**, 728 (2006).
[82] A. B. Arbuzov and E. S. Scherbakova, JETP Lett. **83**, 427 (2006).
[83] G. Balossini *et al.*, Nucl. Phys. B, Proc. Suppl. **162**, 59 (2006).
[84] G. Balossini *et al.*, Nucl. Phys. **B758**, 227 (2006).
[85] J. Fleischer *et al.*, Eur. J. Phys. **48**, 35 (2006).
[86] J. Blumlein and S. Klein, Proc. Sci., ACAT (2007) 084 [arXiv:0706.2426].
[87] K. Mönig, Bhabha Workshop of SFB/TRR 9 on Bhabha scattering at the ILC, Karlsruhe, 2005, http://sfb-tr9.particle.uni-karlsruhe.de/veranstaltungen/bhabha-talks/moenig.pdf.
[88] A. Denig, Bhabha Workshop of SFB/TRR 9 on Bhabha scattering at Dafne: The Kloe luminosity measurement, Karlsruhe, 2005, http://sfb-tr9.particle.uni-karlsruhe.de/veranstaltungen/bhabha-talks/denig.pdf.
[89] L. Trentadue, Bhabha Workshop of SFB/TRR 9 on Measurement of α_{QED}: An alternative approach,

Karlsruhe, 2005, http://sfb-tr9.particle.uni-karlsruhe.de/veranstaltungen/bhabha-talks/trentadue.pdf.
[90] S. Jadach, Bhabha Workshop of SFB/TRR 9 on Theoretical calculations for LEP luminosity measurements, Karlsruhe, 2005, http://sfb-tr9.particle.uni-karlsruhe.de/veranstaltungen/bhabha-talks/jadach.pdf.
[91] G. Balossini *et al.*, Acta Phys. Pol. B **38**, 3441 (2007).
[92] G. Balossini *et al.*, arXiv:0806.4909.
[93] S. Actis, M. Czakon, J. Gluza, and T. Riemann, Phys. Rev. Lett. **100**, 131602 (2008).
[94] V. Smirnov, Phys. Lett. B **524**, 129 (2002).
[95] Z. Bern, L. Dixon, and A. Ghinculov, Phys. Rev. D **63**, 053007 (2001).
[96] N. Glover, B. Tausk, and J. van der Bij, Phys. Lett. B **516**, 33 (2001).
[97] R. Bonciani, P. Mastrolia, and E. Remiddi, Nucl. Phys. **B676**, 399 (2004).
[98] R. Bonciani *et al.*, Nucl. Phys. **B681**, 261 (2004).
[99] R. Bonciani, P. Mastrolia, and E. Remiddi, Nucl. Phys. **B661**, 289 (2003).
[100] R. Bonciani *et al.*, Nucl. Phys. **B716**, 280 (2005).
[101] M. Czakon, J. Gluza, and T. Riemann, Nucl. Phys. B, Proc. Suppl. **135**, 83 (2004).
[102] M. Czakon, J. Gluza, and T. Riemann, Phys. Rev. D **71**, 073009 (2005).
[103] G. Heinrich and V. Smirnov, Phys. Lett. B **598**, 55 (2004).
[104] A. A. Penin, Phys. Rev. Lett. **95**, 010408 (2005).
[105] A. A. Penin, Nucl. Phys. **B734**, 185 (2006).
[106] R. Bonciani and A. Ferroglia, Phys. Rev. D **72**, 056004 (2005).
[107] M. Czakon, J. Gluza, and T. Riemann, Acta Phys. Pol. B **36**, 3319 (2005).
[108] R. Bonciani and A. Ferroglia, Nucl. Phys. B, Proc. Suppl. **157**, 11 (2006).
[109] M. Czakon, J. Gluza, and T. Riemann, Nucl. Phys. **B751**, 1 (2006).
[110] A. Mitov and S. Moch, J. High Energy Phys. 05 (2007) 001.
[111] S. Actis, M. Czakon, J. Gluza, and T. Riemann, Nucl. Phys. B, Proc. Suppl. **160**, 91 (2006).
[112] T. Becher and K. Melnikov, J. High Energy Phys. 06 (2007) 084.
[113] S. Actis *et al.*, Nucl. Phys. **B786**, 26 (2007).
[114] S. Actis *et al.*, Acta Phys. Pol. B **38**, 3517 (2007).
[115] S. Actis *et al.*, XXXI Conference on Matter to the Deepest, Ustroń, Poland, 2007, http://prac.us.edu.pl/~us2007/talks.htm.
[116] R. Bonciani, A. Ferroglia, and A. A. Penin, Phys. Rev. Lett. **100**, 131601 (2008).
[117] J. Fleischer *et al.*, Acta Phys. Pol. B **38**, 3529 (2007).
[118] R. Bonciani, A. Ferroglia, and A. A. Penin, J. High Energy Phys. 02 (2008) 080.
[119] J. H. Kuhn and S. Uccirati, arXiv:0807.1284.
[120] DESY, webpage http://www-zeuthen.desy.de/theory/research/bhabha/bhabha.html.
[121] W.-M. Yao *et al.* (Particle Data Group), J. Phys. G **33**, 1 (2006).
[122] N. Cabibbo and R. Gatto, Phys. Rev. **124**, 1577 (1961).
[123] R. E. Cutkosky, J. Math. Phys. (N.Y.) **1**, 429 (1960).
[124] B. Kniehl *et al.*, Phys. Lett. B **209**, 337 (1988).
[125] T. van Ritbergen and R. G. Stuart, Phys. Lett. B **437**, 201 (1998).
[126] M. Steinhauser, Phys. Lett. B **429**, 158 (1998).
[127] S. Eidelman and F. Jegerlehner, Z. Phys. C **67**, 585 (1995).
[128] H. Burkhardt and B. Pietrzyk, Phys. Rev. D **72**, 057501 (2005).
[129] F. Jegerlehner, Nucl. Phys. B, Proc. Suppl. **162**, 22 (2006).
[130] K. Hagiwara *et al.*, Phys. Lett. B **649**, 173 (2007).
[131] G. Kallen and A. Sabry, Kong. Dan. Vid. Sel. Mat. Fys. Med. **29N17**, 1 (1955).
[132] F. Jegerlehner, Fortran program hadr5.f (version 02 Nov 2003), available at http://www-com.physik.hu-berlin.de/fjeger.
[133] H. Burkhardt, Report No. TASSO-NOTE-192 (1981), and Fortran program repi.f (1986).
[134] D. Maitre, Comput. Phys. Commun. **174**, 222 (2006).
[135] D. Maitre, arXiv:hep-ph/0703052.
[136] R. Barbieri, J. A. Mignaco, and E. Remiddi, Nuovo Cimento Soc. Ital. Fis. A **11**, 824 (1972).
[137] R. Barbieri, J. A. Mignaco, and E. Remiddi, Nuovo Cimento Soc. Ital. Fis. A **11**, 865 (1972).
[138] G. Burgers, Phys. Lett. **164B**, 167 (1985).
[139] S. Actis, J. Gluza, and T. Riemann, arXiv:0807.0174.
[140] J. Gluza, K. Kajda, and T. Riemann, Comput. Phys. Commun. **177**, 879 (2007).
[141] M. Czakon, Comput. Phys. Commun. **175**, 559 (2006).
[142] J. Frenkel and J. C. Taylor, Nucl. Phys. **B116**, 185 (1976).
[143] M. Melles, Acta Phys. Pol. B **28**, 1159 (1997).
[144] S. Jadach, B. F. L. Ward, and Z. Was, Comput. Phys. Commun. **130**, 260 (2000).
[145] M. Kobel *et al.* (Two Fermion Working Group), arXiv:hep-ph/0007180.
[146] R. Bonciani *et al.*, Nucl. Phys. **B701**, 121 (2004).
[147] J. Fleischer *et al.*, Eur. Phys. J. C **31**, 37 (2003).
[148] M. Davier *et al.*, Eur. Phys. J. C **27**, 497 (2003).
[149] S. R. Amendolia *et al.* (NA7), Nucl. Phys. **B277**, 168 (1986).
[150] Fortran routine, private communications with T. Teubner. The Fortran program is based on the data compilation performed for [130,151]. The publication is in preparation. The routine is available upon request from the authors, Emails: dnomura@post.kek.jp, thomas.teubner@liverpool.ac.uk. We used version of 2008-04-26.
[151] K. Hagiwara, A. D. Martin, D. Nomura, and T. Teubner, Phys. Rev. D **69**, 093003 (2004).
[152] R. V. Harlander and M. Steinhauser, Comput. Phys. Commun. **153**, 244 (2003).
[153] G. 't Hooft and M. Veltman, Nucl. Phys. **B153**, 365 (1979).
[154] J. Vollinga and S. Weinzierl, Comput. Phys. Commun. **167**, 177 (2005).
[155] R. Crandall, Note on fast polylogarithm computation, 2006, http://people.reed.edu/~crandall/papers/Polylog.pdf.
[156] U. Langenfeld (private communication).
[157] J. A. M. Vermaseren, Comput. Phys. Commun. **83**, 45 (1994).
[158] D. Binosi and L. Theussl, Comput. Phys. Commun. **161**, 76 (2004).